Eur. Phys. J. C 24, 469–483 (2002)
Digital Object Identifier (DOI) 10.1007/s10052-002-0965-3

THE EUROPEAN PHYSICAL JOURNAL C

Analysis and interpretation of new low-energy $\pi\pi$ scattering data

S. Descotes[1,a], N.H. Fuchs[2,b], L. Girlanda[3,c], J. Stern[4,d]

[1] Department of Physics and Astronomy, University of Southampton, Southampton SO17 1BJ, UK
[2] Department of Physics, Purdue University, West Lafayette IN 47907, USA
[3] Dipartimento di Fisica, Università di Padova and INFN, Via Marzolo 8, 35131 Padova, Italy
[4] Groupe de Physique Théorique, Institut de Physique Nucléaire, 91406 Orsay-Cedex, France

Received: 11 December 2001 / Revised version: 28 March 2002 /
Published online: 7 June 2002 –

Abstract. The recently published E865 data on charged K_{e4} decays and $\pi\pi$ phases are reanalyzed to extract values of the two S-wave scattering lengths, of the subthreshold parameters α and β, of the low-energy constants $\bar{\ell}_3$ and $\bar{\ell}_4$ as well as of the main two-flavour order parameters: $\langle\bar{u}u\rangle$ and F_π in the limit $m_u = m_d = 0$ taken at the physical value of the strange quark mass. Our analysis is exclusively based on direct experimental information on $\pi\pi$ phases below 800 MeV and on the new solutions of the Roy equations by Ananthanarayan et al. The result is compared with the theoretical prediction relating $2a_0^0 - 5a_0^2$ and the scalar radius of the pion, which was obtained in two-loop Chiral Perturbation Theory. A discrepancy at the 1-σ level is found and commented upon.

1 Introduction

Recently, a new measurement of K_{e4}^+ decay and of the $\pi\pi$ phase shift difference $\delta_0^0 - \delta_1^1$ has been published [1] by the Brookhaven E865 collaboration. New low-energy $\pi\pi$ scattering data constitute a rare event which has not happened since the last Geneva-Saclay experiment 25 years ago [2], and the corresponding determination of the isoscalar S-wave scattering length $a_0^0 = 0.26 \pm 0.05$. The new experiment [1] improves the statistics by more than a factor of 10, and the outcome for a_0^0 is not only more accurate, but also points towards a smaller central value as expected by the standard version of Chiral Perturbation Theory (χPT) [3]. It is crucial to know the two S-wave scattering lengths a_0^0 and a_0^2 as precisely as possible and to avoid confusing their model-independent extraction from the data on one hand with theoretical χPT-based predictions on the other hand. This is the main purpose of the present paper. The principal model-independent tools of our analysis are Roy equations [4] and their recent solution by Ananthanarayan, Colangelo, Gasser and Leutwyler (ACGL) [5]. In a suitable kinematical range, Roy equations represent a rigorous consequence of general properties of the scattering amplitude: analyticity, unitarity, crossing symmetry and asymptotic bounds. The ACGL solution uniquely fixes the three phases relevant at low energies, $\delta_0^0(E), \delta_1^1(E), \delta_0^2(E)$ for $E < E_0 = 800$ MeV in terms of the two scattering lengths a_0^0 and a_0^2, and experimental data above $s_0 = E_0^2$. In this way, sufficiently precise data on phase shifts for $2M_\pi < E < E_0$ can be converted into a model-independent determination of the two S-wave scattering lengths. Conversely, the knowledge of a_0^0 and a_0^2 allows one to determine any other low-energy $\pi\pi$ observables which might be needed for a theoretical interpretation of experimental results in terms of the chiral structure of QCD vacuum. Unfortunately, the combination $\delta_0^0 - \delta_1^1$ near threshold (which is measured in K_{e4} experiments) is not strongly sensitive to a_0^2, for a given a_0^0, even if the former is allowed to vary over the whole Universal Band (UB). This can be seen explicitly, for instance, from the ACGL solutions of Roy equations. We will show (Sect. 3) that a model-independent and relatively accurate determination of both S-wave scattering lengths is nevertheless possible, if the existing K_{e4} data on $\delta_0^0 - \delta_1^1$ are combined with the older production data by Hoogland et al. [6] and by Losty et al. [7], concerning the $I = 2$ S-wave for $E < 800$ MeV. Our result reads $a_0^0 = 0.228 \pm 0.012$, $a_0^2 = -0.0382 \pm 0.0038$. Subsequently (Sect. 4), Roy equations will be used once more to convert the S-wave scattering lengths into the determination of the subthreshold parameters α and β (as well as $\lambda_1 \ldots \lambda_4$) introduced in [8] and under a different name ($b_1 \ldots b_6$) in [9]. The expansion of the parameters α and β in powers of quark mass converges more rapidly than in the case of scattering lengths. The knowledge of subthreshold param-

[a] e-mail: sdg@hep.phys.soton.ac.uk
[b] e-mail: nhf@physics.purdue.edu
[c] e-mail: luca.girlanda@pd.infn.it
[d] e-mail: stern@ipno.in2p3.fr

eters is therefore used to extract the low-energy constants (LEC's) $\bar{\ell}_3$ and $\bar{\ell}_4$, as well as the main two-flavour order parameters (Sects. 5 and 6). All this analysis is based on existing solutions of Roy equations as given by ACGL in [5]. In parallel, we construct an extended solution of Roy equations, incorporating the dependence on the value of phase shifts at the matching point $E_0 = 800$ MeV. This allows the control of the propagation of errors arising from the intermediate energy data, which was not possible using the published ACGL solution of [5]. Finally, our model-independent determination of scattering lengths and other low-energy parameters is compared with the theoretical prediction of the tight correlation between $2a_0^0 - 5a_0^2$ and the scalar radius of the pion $\langle r^2\rangle_s$ [10]. If the latter prediction is combined with the E865 data alone [1], one obtains $a_0^0 = 0.218 \pm 0.013$, $a_0^2 = -0.0449 \pm 0.0033$ assuming the value of the scalar radius $\langle r^2\rangle_s = 0.61 \pm 0.04\text{fm}^2$. Our simultaneous fit to the K_{e4} [1,2] and to the high-energy $\pi^+\pi^+$-production data [6,7] suggests a discrepancy at the 1-σ level with the two-loop χPT prediction for $2a_0^0 - 5a_0^2$ [10]. We point out that the treatment of symmetry breaking $O(p^6)$ corrections in the scalar channel might be at the origin of this discrepancy (Sect. 7).

2 Theoretical motivation

Before we proceed further it may be useful to summarize briefly the main theoretical motivations which drive our interest in accurate low-energy $\pi\pi$ scattering experiments, eventually completed by independent experimental information of a different kind. In particular it is worth explaining why a small difference in the values of scattering lengths like the one mentioned in the introduction may be relevant. The reader who is mostly interested in the analysis and less in the interpretation of the new data can skip this section and proceed directly to the following one. Nothing in our analysis depends on theoretical ideas summarized here.

During the last two years our understanding of the pattern of chiral symmetry breaking in QCD has considerably evolved [11–16], in particular concerning the dynamical role of the number of light flavours. $\pi\pi$ scattering provides important information about the $SU(2) \times SU(2)$ chiral structure of QCD vacuum in the limit of massless u and d quarks. The theoretical interpretation of this information, however, remains incomplete unless one learns how to disentangle the influence of the strange quark. If the strange quark were massless, we deal with $SU(3) \times SU(3)$ symmetry, which is the theoretician's paradise [17]. The reason is that all remaining quarks (c, b, t) are heavy compared to the QCD scale, and consequently their influence on the chiral structure of the vacuum remains tiny. For the same reason, we would reach another (a priori different) paradise if the strange quark mass were sent to infinity. In these two limiting cases, the question of the pattern of chiral symmetry breaking reduces to the question of condensation of massless $\bar{q}q$ pairs in the vacuum; $\pi\pi$ scattering would by itself suffice to detect and fully control this one-fermion loop effect. Unfortunately, the deplorable fact that we live in neither of these paradises [17] complicates the problem a bit. In the real world the strange quark is considerably heavier than u and d quarks and yet it is light compared to the QCD scale. Consequently, the vacuum gets polluted by *massive* virtual $\bar{s}s$ pairs. One may wonder how this fact could affect the $SU(2) \times SU(2)$ chiral structure of the vacuum, which is merely a matter of massless u and d quarks. Indeed, there would be no such effect in the large-N_c limit, in which the transition:

$$\bar{s}s \longleftrightarrow \bar{u}u + \bar{d}d \tag{1}$$

is forbidden and, consequently, strange and non-strange virtual pairs remain uncorrelated. Today we know that in the real world, the OZI-rule violating transition (1) is in fact rather important precisely in the vacuum channel [14] and that the resulting symmetry breaking correlation $\langle\bar{s}s(\bar{u}u+\bar{d}d)\rangle$ affects the $SU(2)\times SU(2)$ chiral structure of the vacuum. We call this phenomenon which proceeds via at least two fermion loops *the induced quark condensate* [16]. It is proportional to m_s, it enhances the effect of the genuine condensate of massless quarks characteristic of the ideal world with $SU(3) \times SU(3)$ symmetry, and it would persist even if the latter would be absent. The situation can be summarized by the formula:

$$\Sigma(2) = \Sigma(3) + m_s Z_{\text{scalar}}\,, \tag{2}$$

where $\Sigma(N_f)$ denotes the v.e.v. $-\langle\bar{u}u\rangle$ of the lightest quark in the limit in which the first N_f quarks become massless, whereas the second term represents the induced condensate with $Z_{\text{scalar}} > 0$ proportional to the amplitude of the transition (1) in the scalar channel. Since $\Sigma(3)$ is defined in the limit $m_u = m_d = m_s = 0$ and since there are no more massive quarks left which would be sufficiently light to pollute the vacuum, $\Sigma(3) = F_0^2 B_0$ (in the current χPT notation) represents the true condensate of massless quarks of the $SU(3) \times SU(3)$ symmetric world. On the other hand, $\Sigma(2)$, defined at $m_u = m_d = 0$ and the physical value of m_s, is detected in low energy $\pi\pi$ scattering. Our original quest for the importance of quark condensation [18,19] did not sufficiently emphasize the subtlety of the theoretical and experimental distinction between $\Sigma(2)$ and $\Sigma(3)$. Phenomenological indications in favour of a substantial OZI-rule violating transition, (1), were not yet available and the large-N_c wisdom $\Sigma(2) \sim \Sigma(3)$ dominated our thinking. Today, we have to answer the more precise question whether the suppression of the quark condensate – expected in QCD due to the screening effect of multiflavour massless quark loops – is already visible for $N_f = 3$.

The important consequence of the new E865 data [1] is that $\Sigma(2)$ is sufficiently large to keep the two-flavour GOR ratio $X(2) = (m_u + m_d)\Sigma(2)/F_\pi^2 M_\pi^2$ close to one [20] (see Sect. 6 for more details). However, we still do not know whether the observed size of $\Sigma(2)$ reflects an important contribution of the genuine condensate $\Sigma(3)$ or whether it is (at least partially) due to the induced condensate and to the strange quark mass, i.e. to the second term in (2). In the latter case, the genuine condensate $\Sigma(3)$ could be rather small and the corresponding three-flavour GOR

ratio $X(3) = (m_u + m_d)\Sigma(3)/F_\pi^2 M_\pi^2$ significantly below one. [Since $X(2) \sim 1$, the suppression of $X(3)$ would imply an important contribution of m_s to M_π^2 through terms $mm_s, mm_s^2 \ldots$, where $m = (m_u + m_d)/2$.] Moussallam [12] has proposed a rapidly convergent sum rule that allows an estimate of the transition (1) and of the size of the induced condensate. Detailed studies of this sum rule [12,13,15] are compatible with a suppression of the condensate by a factor ~ 2 when going from 2 to 3 flavours: $X(3) \sim X(2)/2$ indicating that the two contributions to $\Sigma(2)$ on the right-hand side of (2) should be of comparable size. It is rather difficult to make a precise quantitative statement here: the evaluation of the Moussallam's sum rule involves a few steps that include some unproved properties of the scalar form-factors and a certain model-dependence (of a similar type to the one in the phenomenological evaluation of the scalar radius of the pion [21]). Hence, it is crucial to find an independent way of disentangling the genuine and induced condensate contributions to $\Sigma(2)$.

An analysis of $\pi\pi$ scattering exclusively based on $SU(2) \times SU(2)$ χPT can never separate the two components of $\Sigma(2)$ in (2), for the simple reason that it does not involve any information on the actual size of m_s. On the other hand, an $SU(3) \times SU(3)$ analysis of suitable $\pi\pi$ observables supplemented by additional observables, such as M_K or F_K, directly sensitive to m_s, can considerably restrict the possible values of three important parameters: *i)* the three-flavour GOR ratio $X(3) = 2m\Sigma(3)/F_\pi^2 M_\pi^2$, *ii)* the quark mass ratio $r = m_s/m$ and *iii)* the pseudoscalar decay constant $F_0 = F_\pi|_{m_u = m_d = m_s = 0}$. An example of a relation of this type is the strong correlation which exists between r and $X(2)$ [11,15]. Further restrictions can be obtained from the emerging analysis of $K - \pi$ scattering [22].

We are going to present this combined analysis in a separate paper [23]. It will be shown in particular that in order to be conclusive, one has to use extremely precise values of subthreshold $\pi\pi$ parameters α and β as the input of our analysis. Typically, the actual precision driven by the new E865 data analyzed in the following section will be just sufficient to reach conclusions about the suppression of the genuine condensate $X(3)$ on the 1-σ level. Notice that a more precise measurement of low-energy $\pi\pi$ scattering is conceivable in more dedicated experiments which are either ongoing [24] or planned [25].

3 The two S-wave scattering lengths

3.1 Extended solutions of Roy equations

The E865 data can be analyzed using a parametric representation of the solution of Roy equations for the $\pi\pi$ phase shifts. A set of dispersion relations derived by Roy [4] allows one to relate the phase shifts δ_0^0, δ_1^1 and δ_0^2 in the region $4M_\pi^2 \le s \le s_0$ (with $\sqrt{s_0} \sim 0.8$ GeV) to data at intermediate energies ($\sqrt{s_0} \le \sqrt{s} \le 2$ GeV) and to two subtraction constants. The latter can be identified with the two S-wave scattering lengths a_0^0 and a_0^2.

The Roy equations, analyzed thoroughly in [5], yield a boundary value problem. The solutions must interpolate between the phase shifts at the threshold, fixed by a_0^0 and a_0^2, and the three phases at the matching point s_0:

$$\theta_0 = \delta_0^0(s_0), \qquad \theta_1 = \delta_1^1(s_0), \qquad \theta_2 = \delta_0^2(s_0), \quad (3)$$

determined from data above s_0. As stated in [5], the behaviour of the phases above s_0 is less important than the boundary values, because they only affect the slope and the curvature of the solutions. With the experimental input encountered in practice, the system of Roy equations admits a unique solution provided that the matching point s_0 is carefully chosen (0.78 GeV $\le \sqrt{s_0} \le$ 0.86 GeV).

Moreover, for given boundary conditions $(a_0^0, \theta_0, \theta_1, \theta_2)$, arbitrary values of a_0^2 generate a strong cusp in the P-wave solution at the matching point s_0. If we require the phases to be smooth, a_0^2 is determined as a function of $(a_0^0, \theta_0, \theta_1, \theta_2)$. Since $\theta_{0,1,2}$ can only vary in their experimental range, this requirement leads to a correlation between a_0^0 and a_0^2, defining the so-called Universal Band (UB) in the (a_0^0, a_0^2) plane. Different choices for $\theta_{0,1,2}$ represent lines in the UB, $a_0^2 = F(a_0^0)$. Inverting the relation between a_0^2 and $(a_0^0, \theta_0, \theta_1, \theta_2)$, we can consider θ_2 as a function of the other parameters. This means the solutions of the Roy equations do depend eventually on $(a_0^0, a_0^2, \theta_0, \theta_1)$ only.

The data in the $I = 0, 1$ channels lead to:

$$\theta_0 = 82.3^\circ \pm 3.4^\circ, \qquad \theta_1 = 108.9^\circ \pm 2^\circ. \quad (4)$$

The authors of [5] have provided explicit numerical solutions of the Roy equations for $\theta_0 = 82.0^\circ$ and $\theta_1 = 108.9^\circ$. We have included in the parametrization of Roy equations' solutions[1], an explicit dependence on θ_0 and θ_1, generating solutions (with the same driving terms and experimental input above the matching point s_0) for nine different sets (θ_0, θ_1) and a few tens of (a_0^0, a_0^2) inside the UB.

Following [5], we parametrize our solutions, for energies below 800 MeV, as:

$$\tan\delta_\ell^I(s) = \sqrt{1 - \frac{4M_\pi^2}{s}} q^{2\ell} \left\{ A_\ell^I + B_\ell^I q^2 + C_\ell^I q^4 + D_\ell^I q^6 \right\} \times \left(\frac{4M_\pi^2 - s_\ell^I}{s - s_\ell^I} \right). \quad (5)$$

The dependence on a_0^0 and a_0^2 of the Schenk parameters $X = A, B, C, D$ in (5) is well approximated by:

$$X_\ell^I = z_1 + z_2 u + z_3 v + z_4 u^2 + z_5 v^2 + z_6 uv + z_7 u^3 + z_8 u^2 v + z_9 u v^2 + z_{10} v^3, \quad (6)$$

where:

$$u = \frac{a_0^0}{p_0} - 1, \quad v = \frac{a_0^2}{p_2} - 1, \quad p_0 = 0.225, \quad p_2 = -0.03706, \quad (7)$$

[1] We have used the standard routines of MINUIT for all the minimization and fitting procedures of this paper

while, for each coefficient z_i, the dependence on the phase shifts at the matching point is parametrized by:

$$z_j = a_j + \delta\theta_0\, b_j + \delta\theta_1\, c_j\,, \tag{8}$$

where

$$\delta\theta_0 = \theta_0 - 82.3^\circ\,, \qquad \delta\theta_1 = \theta_1 - 108.9^\circ\,. \tag{9}$$

The parameters s_0^0, s_1^1 and s_0^2 are fixed by the boundary conditions:

$$\delta_0^0(s_0) \equiv \theta_0\ , \qquad \delta_1^1(s_0) \equiv \theta_1\ , \qquad \delta_0^2(s_0) \equiv \theta_2\ , \tag{10}$$

where $\theta_2(a_0^0, a_0^2, \theta_0, \theta_1)$ is parametrized following (6) and (8). The coefficients a_j, b_j, c_j are collected in Appendix B. This parametrization describes our solutions to better than 0.3° for the $I = 0, 2$, and 0.5° for the $I = 1$ partial waves in the Universal band.

By setting $\theta_0 = 82.0^\circ$ and $\theta_1 = 108.9^\circ$, we can compare with [5]. We obtain slightly different Schenk parameters for the so-called reference point $a_0^0 = 0.225$ and $a_0^2 = -0.0371$, but the phase shifts are identical up to a few tenths of a degree. We obtain the same Universal Band, and only its lower half meets the consistency condition (Roy equations fulfilled in their range of validity $2M_\pi \le \sqrt{s} \le \sqrt{s_1} = 1.15$ GeV). In the range of interest for a_0^0, the gap between the parametrization of [5] and our Roy solutions is at most 0.3° in the $I = 0, 2$ channels and 0.7° in the $I = 1$ channel (for $\sqrt{s} \sim 0.7$ GeV and much smaller near threshold in all the channels).

3.2 Model-independent determination of a_0^0 and a_0^2

The E865 data on $\delta_0^0 - \delta_1^1$ were analyzed in [1] in order to extract a_0^0. While two different (although compatible) results were quoted in this reference for a_0^0, ($a_0^0 = 0.228 \pm 0.012 \pm 0.004^{+0.006}_{-0.012}$ and $a_0^0 = 0.216 \pm 0.013 \pm 0.004 \pm 0.005$), no results were given for a_0^2, which is harder to pin down from K_{e4} data alone (see Sect. 1). An unconstrained fit of E865 data, using the Roy equations of [5], leads to a rather inaccurate result for the $I = 2$ scattering length: $a_0^0 = 0.237 \pm 0.033$ and $a_0^2 = -0.0305 \pm 0.0226$ ($\chi^2 = 5.44/5$ d.o.f and the correlation coefficient is 0.96).

In order to extract both scattering lengths additional information has to be provided. The first constraint arises from the necessary consistency of the Roy solutions with the $I = 2$ data above the matching point. This forces the S-wave scattering lengths to lie within the so-called Universal Band. Unfortunately, this model-independent constraint is rather weak.

We make use of additional information by fitting a broader set of data below 800 MeV, namely Rosselet and E865 sets for $I = 0, 1$ [2,1] and Hoogland (sol. A) and Losty sets for $I = 2$ [6,7]. Notice that a similar fit has been considered in [5,26] but without the E865 data (cf. Figs. 11 and 12 in [5]).

We first perform a fit using the solutions of the Roy equations of [5]. The χ^2 is defined as:

$$\chi^2_{\rm global}(a_0^0, a_0^2) = \sum_{j=1}^{9} \left(\frac{(\delta_0^2)^{\rm ACGL}(s_j^{\rm exp}) - (\delta_0^2)_j^{\rm exp}}{\sigma_j^{\rm exp}} \right)^2 + \sum_{i=1}^{11} \left(\frac{[\delta_0^0 - \delta_1^1]^{\rm ACGL}(s_i^{\rm exp}) - [\delta_0^0 - \delta_1^1]_i^{\rm exp})}{\sigma_i^{\rm exp}} \right)^2, \tag{11}$$

where $[\delta_\ell^I]^{\rm ACGL}(a_0^0, a_0^2, s)$ is the parametrization of Roy solutions proposed in [5]. i and j are the indices of the experimental points for $I = (0, 1)$ and $I = 2$ respectively. This fitting procedure, referred to as "global", yields:

$$\text{Global}: \quad a_0^0 = 0.228 \pm 0.012, \quad a_0^2 = -0.0382 \pm 0.0038. \tag{12}$$

with $\chi^2_{\rm min} = 16.45/18$ d.o.f and a correlation coefficient of 0.788. Including data on the P-wave below 800 MeV reported by Protopopescu et al. [27] does not change the result of the fit, yielding[2] $\chi^2_{\rm min} = 23.1/28$ d.o.f. and $a_0^0 = 0.228 \pm 0.012$, $a_0^2 = -0.0392 \pm 0.0038$.

A second fitting procedure can be followed, in which we use our solutions of the Roy equations to include the dependence on the phase shifts at the matching point (θ_0, θ_1). The χ^2 is then defined as:

$$\chi^2_{\rm extended}(a_0^0, a_0^2, \theta_0, \theta_1) = \sum_{j=1}^{9} \left(\frac{(\delta_0^2)^{\rm ext}(s_j^{\rm exp}) - (\delta_0^2)_j^{\rm exp}}{\sigma_j^{\rm exp}} \right)^2 + \sum_{i=1}^{11} \left(\frac{[\delta_0^0 - \delta_1^1]^{\rm ext}(s_i^{\rm exp}) - [\delta_0^0 - \delta_1^1]_i^{\rm exp})}{\sigma_i^{\rm exp}} \right)^2 + \left(\frac{\theta_0 - 82.3^\circ}{3.4^\circ} \right)^2 + \left(\frac{\theta_1 - 108.9^\circ}{2^\circ} \right)^2, \tag{13}$$

where $[\delta_\ell^I]^{\rm ext}(a_0^0, a_0^2, \theta_0, \theta_1, s)$ is our extended parametrization of Roy solutions. This fit, called "extended", leads to the same S-wave scattering lengths as the "global" fit:

$$\text{Extended}: a_0^0 = 0.228 \pm 0.013,\ a_0^2 = -0.0380 \pm 0.0044, \quad \theta_0 = 82.1^\circ \pm 3.3^\circ, \quad \theta_1 = 108.9^\circ \pm 2.0^\circ \tag{14}$$

with $\chi^2_{\rm min} = 16.48/18$ d.o.f and the correlation matrix:

	a_0^0	a_0^2	θ_0	θ_1
a_0^0	1.000	0.799	−0.319	−0.004
a_0^2	–	1.000	−0.271	0.029
θ_0	–	–	1.000	0.000
θ_1	–	–	–	1.000

(15)

The results of these analyses are shown in Fig. 1, where we have indicated the 1- and 2-σ contours for both determinations. These contours are defined respectively as[3] $\chi^2 = \chi^2_{\rm min} + 1$ and $\chi^2 = \chi^2_{\rm min} + 4$. We see that our fitting result lies slightly below the center of the UB, where the consistency condition for Roy equations is met.

[2] Specifically we have used the energy-independent solution, which has larger error bars. The P-wave production data at low energy have been often criticized, most recently in [5]. Therefore we prefer not to include them in the analysis, but instead use our results to predict the P-wave at low energy

[3] We recall that in the case of the simultaneous determination of two variables, this definition of the contours correspond to 39% and 86% confidence level

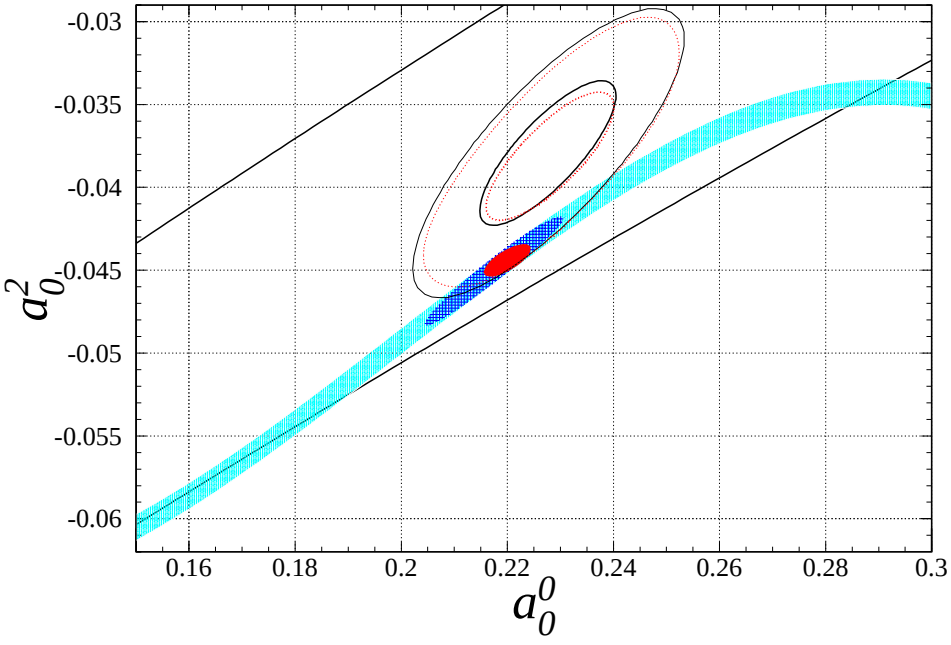

Fig. 1. Fit results using either the Roy solutions of [5] (red, dotted ellipse – "global") or our parameterization of the Roy solutions (black, solid ellipse – "extended"). In each case, the thicker lines indicate the 1-σ ellipse, and the thinner ones the 2-σ contour. The Universal Band (delimited by the two straight lines) is drawn according to [5], and the narrow strip (shaded region, cyan) related to the scalar radius of the pion is taken from [10]. We have indicated the result of the fit "scalar" (blue, hatched ellipse) and the SχPT prediction of [29] (red, filled small ellipse)

A comment is in order here concerning our use of the ACM(A) $I = 2$ phase shifts by Hoogland et al. These were extracted following the method A, which is a conventional Chew-Low extrapolation to the pion pole of the measured t-channel ($m = 0$) helicity moments [6] (the beam momentum was 14 GeV/c). A similar method was used by Losty et al. [7]. A second method (B) is presented in [6], which is based on an overall fit of an (absorption) model for the amplitude to all non-negligible s-channel helicity moments ($m = 0$ and $m = 1$). The method B involves extra assumptions and parameters, some of which exhibit unexpectedly rapid energy variations. No χ^2 is given in [6] (in a preliminary analysis [28], based on a third of the data, a poor χ^2 was reported for method B).

We have tried to use in our fit solution B of [6] instead of solution A. Due to the small error bars of the former, we did not succeed in obtaining a consistent description of both ACM(B) and E865-K_{e4} data within the ACGL solutions of Roy equations [5]. The minimum has $\chi^2 = 68/18$ d.o.f. and is situated far outside the Universal Band. Such a fit has little meaning, since the ACGL solutions are valid exclusively inside the Universal Band. Solution ACM(A) is free from such difficulties.

It has been suggested in [5] that the difference between the phase shifts ACM(A) and (B) indicates sizeable systematic errors, and that the errors associated with ACM(A) solution should consequently be enlarged. It is not obvious to us that method B yields a correct estimate of the systematic errors inherent to method A – especially since the two methods do not use the same sample of data. We find it nevertheless useful to show in Appendix A and in Fig. 6 how our results would be modified if the errors in ACM(A) phase shifts were increased according to the prescription advocated in [5]. Let us mention here that these modifications barely affect the main conclusion.

3.3 Comparison with the χPT prediction for $2a_0^0 - 5a_0^2$

In the theoretical prediction of a_0^0 and a_0^2 based on standard χPT including $O(p^6)$ accuracy [9,10,20,29], one may distinguish two steps. The first step concerns the relation between the combination $2a_0^0 - 5a_0^2$ and the scalar radius of the pion $\langle r^2\rangle_s$ [10,29]. This step is practically independent of the badly known $O(p^4)$ constant $\bar{\ell}_3$ but it requires an independent phenomenological determination of $\langle r^2\rangle_s$ and it is rather sensitive to the two-loop corrections (a more detailed discussion of this theoretical prediction can be found in Sect. 7). If one takes the value $\langle r^2\rangle_s = 0.61 \pm 0.04$ fm^2, the prediction amounts to a narrow strip in the $a_0^0 - a_0^2$ plane, given in [10] and reproduced in Fig. 1:

$$a_0^2 = G(a_0^0) \pm .0008, \tag{16}$$

where the function $G(a_0^0)$ may be parametrized as

$$G(a_0^0) = -.0444 + .236(a_0^0 - .22) - .61(a_0^0 - .22)^2 \\ -9.9(a_0^0 - .22)^3\,, \tag{17}$$

and the error bar is estimated within the theoretical framework defined in [10,29] (see Sect. 7 of the present paper). The second step of the prediction procedure then consists in locating the actual position inside the narrow strip (16) and it involves, among other things, an estimate of the constant $\bar{\ell}_3$.

The analysis performed in the previous subsection makes use only of the E865 and Rosselet data on $\delta_0^0 - \delta_1^1$, the Hoogland and Losty data on δ_0^2 together with the solution of Roy equations, and does not use χPT or a particular value of $\langle r^2\rangle_s$. It provides thus a sensitive experimental test of the theoretical prediction represented by the CGL correlation (16) and (17). It is seen from Fig. 1 that the 1-σ ellipses resulting from both fits "global" and "extended"

are situated outside the CGL narrow strip despite the fact that they are entirely contained within the Universal Band required by the consistency of Roy equations solution. On the other hand, the 2-σ contours intersect the narrow strip. We thus conclude that there is a marginal (1-σ deviation) discrepancy between the theoretical prediction (17) and the result of the "global" and "extended" fits. This discrepancy will be further commented on in Sect. 7.

In order to make the comparison more quantitative, we can perform a fit to the E865 data alone, imposing by hand the correlation described by the narrow strip. A similar fit has been performed in [10], leading to the central value $a_0^0 = 0.218$ (no uncertainty was indicated in that reference). Our fitting procedure is defined by:

$$\chi^2_{\rm scalar}(a_0^0, a_0^2) = \left(\frac{a_0^2 - G(a_0^0)}{.0008}\right)^2 + \sum_{k=1}^{6} \left(\frac{[\delta_0^0 - \delta_1^1]^{\rm ACGL}(s_k^{\rm exp}) - [\delta_0^0 - \delta_1^1]_k^{\rm exp}}{\sigma_k^{\rm exp}}\right)^2, \quad (18)$$

where k runs only through the E865 points. We have obtained:

$$\text{Scalar}: \quad a_0^0 = 0.218 \pm 0.013, \qquad a_0^2 = -0.0449 \pm 0.0033. \quad (19)$$

with $\chi^2_{\rm min} = 5.89/5$ d.o.f., compatible with the results of E865 [1] for a_0^0, and a correlation coefficient of 0.972. The corresponding 1-σ contour is indicated in Fig. 1. We refer to this fit and to the corresponding 1-σ ellipse as "scalar" to be compared with the "global" and "extended" fits. The meaning of χ^2 and of the standard deviation in the "scalar" fit should be taken with caution: The error bar 0.0008 arises from uncertainties in the experimental input, while the theoretical errors inherent in the estimate of $O(p^6)$ corrections are more difficult to quantify. On the other hand, the fits "global" and "extended" are fully based on experimental data and corresponding errors.

Finally, we would like to briefly comment on the Olsson sum rule for $2a_0^0 - 5a_0^2$, as discussed in [5]. This sum rule converges slowly and demands good control over the asymptotic contribution, which is hard to obtain outside specific models. According to the model used for this purpose in [5], the asymptotic contribution to $2a_0^0 - 5a_0^2$ is $O_{\rm as} = 0.102 \pm 0.017$. Even with such small error bar, the final result shown in (11.2) of [5] is consistent with our global fit, which leads to $(2a_0^0 - 5a_0^2)_{\rm global} = 0.647 \pm 0.015$. If the actual error bar in $O_{\rm as}$ is bigger, the impact of the Olsson sum rule on our fit becomes completely negligible.

4 Subthreshold parameters

In the low-energy domain the $\pi\pi$ amplitude is strongly constrained by chiral symmetry, crossing and unitarity. As was first shown in [18], the amplitude depends on only six parameters up to and including terms of order $(p/\Lambda_H)^6$ in the low-energy expansion. In [8], the amplitude was written as:

$$A_{\rm KMSF}(s|t,u) = A^{\rm cut}(s|t,u) + A^{\rm pol}(s|t,u) \quad (20)$$

$$A^{\rm pol}(s|t,u) = \frac{\beta}{F_\pi^2}\left(s - \frac{4M_\pi^2}{3}\right) + \frac{\alpha}{F_\pi^2}\frac{M_\pi^2}{3} + \frac{\lambda_1}{F_\pi^4}(s-2M_\pi^2)^2 + \frac{\lambda_2}{F_\pi^4}\left[(t-2M_\pi^2)^2 + (u-2M_\pi^2)^2\right] + \frac{\lambda_3}{F_\pi^6}(s-2M_\pi^2)^3 + \frac{\lambda_4}{F_\pi^6}\left[(t-2M_\pi^2)^3 + (u-2M_\pi^2)^3\right], \quad (21)$$

where $A^{\rm cut}$ is a known function of the Mandelstam variables s, t, u that collects the unitarity cuts of the amplitude and explicitly depends on $\alpha, \beta, \lambda_1, \lambda_2$.

This amplitude was constructed as the general solution of unitarity, analyticity and crossing symmetry up to and including $O(p^6)$. The six parameters $\alpha, \beta, \lambda_1, \ldots, \lambda_4$ correspond to an expansion of the amplitude in the central region of the Mandelstam triangle, and are therefore called "subthreshold parameters". A complete calculation in the framework of Standard χPT [9] confirmed this result, allowing in addition to relate the six parameters to the quark masses and LEC's of the standard chiral Lagrangian. This last step is crucial to translate the experimental information into knowledge of the LEC's, which parametrize the chiral structure of the vacuum of QCD. The six parameters introduced in [9], $\bar{b}_1, \ldots, \bar{b}_6$, are dimensionless combinations of LEC's in one-to-one (linear) correspondence with $\alpha, \beta, \lambda_1, \ldots, \lambda_4$ of [8], or with $c_1, \ldots, c_6$, subsequently introduced in [20]. Different choices for the set of six subthreshold parameters correspond to different parametrizations of solutions of unitarity, analyticity and crossing symmetry constraints, which are equivalent up to $O(p^6)$ and only differ at $O(p^8)$.

On the other hand, the Roy equations allow one to determine the low-energy amplitude in terms of only two subtraction constants, identified with the two scalar scattering lengths. It is therefore possible to match the two amplitudes in their common domain of validity, in order to determine, through the experimental determination of the scattering lengths, the six subthreshold parameters. Such a program was already advocated in [30], leading to rapidly convergent sum rules for the parameters $\lambda_1, \ldots, \lambda_4$. A similar matching procedure, using new solutions of the Roy equations, has been carried out in [29] (subtracting the dispersion integrals at $s = 0$). Let us briefly outline the various steps, using the notation and results of this last reference.

Starting with particular values of a_0^0 and a_0^2, we can use the solutions of the Roy equations to compute the low-energy moments J_n^I. In conjunction with the background moments I_n^I and H, estimated in [5], we compute the phenomenological moments $\bar{I}_n^I$ and their linear combinations denoted $\bar{p}_{i=1\ldots6}$ and defined in (3.5) of [29]. Matching the phenomenological and the chiral representations of the amplitude connects the phenomenological parameters $\bar{p}_{i=1\ldots6}$ and the chiral ones $c_{i=1\ldots6}$ [see (4.2) of the same reference]. Appendix A and B of [29] can then be used to translate the chiral parameters $c_{i=1\ldots6}$ into the parameters $\bar{b}_{i=1\ldots6}$ defined in [9], and finally into α, β and $\lambda_{i=1\ldots4}$.

Table 1. Subthreshold parameters for the three different fits considered in this paper. See the text for a discussion of the error bars

	Global	Extended	Scalar
$\bar{b}_1$	-2.08 ± 6.12	-1.51 ± 7.01	-13.06 ± 5.31
$\bar{b}_2$	9.35 ± 1.43	8.93 ± 1.62	11.51 ± 0.62
$\bar{b}_3$	-0.38 ± 0.03	-0.36 ± 0.07	-0.33 ± 0.01
$\bar{b}_4$	0.716 ± 0.008	0.710 ± 0.010	0.727 ± 0.005
$\bar{b}_5$	3.21 ± 0.25	3.21 ± 0.44	3.53 ± 0.15
$\bar{b}_6$	2.23 ± 0.07	2.20 ± 0.08	2.34 ± 0.03
α	1.381 ± 0.242	1.384 ± 0.267	1.034 ± 0.248
β	1.081 ± 0.023	1.077 ± 0.025	1.116 ± 0.010
$\rho_{\alpha\beta}$	-0.14	-0.23	0.53
$\lambda_1 \cdot 10^3$	-4.40 ± 0.28	-4.18 ± 0.63	-3.97 ± 0.12
$\lambda_2 \cdot 10^3$	9.04 ± 0.10	8.96 ± 0.12	9.17 ± 0.06
$\lambda_3 \cdot 10^4$	2.21 ± 0.10	2.22 ± 0.16	2.32 ± 0.06
$\lambda_4 \cdot 10^4$	-1.40 ± 0.04	-1.38 ± 0.04	-1.46 ± 0.02

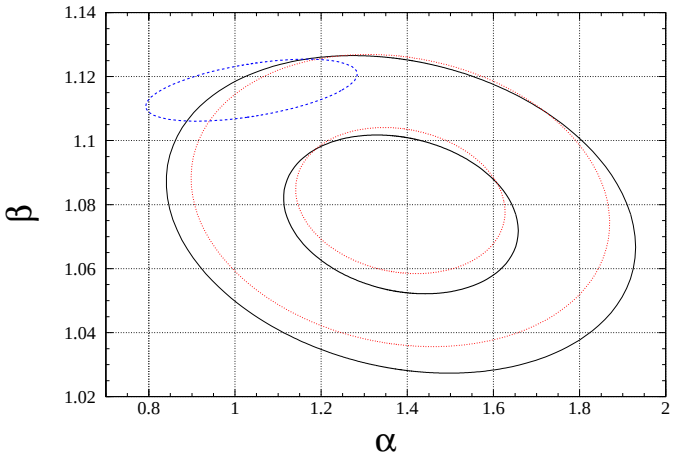

Fig. 2. Correlation between α and β from the fit "scalar" (blue, dashed ellipse) and our fits (black, solid for the "extended" and red, dotted for the "global"). The thicker lines correspond to the 1-σ ellipses, whereas the thinner ones indicate the 2-σ ellipses (not shown for the "scalar" fit)

We can repeat this procedure for each set of (a_0^0, a_0^2), as determined from the "global" and "scalar" fits, or $(a_0^0, a_0^2, \theta_0, \theta_1)$, as determined from the "extended" fit, described in the previous section. In order to take full account of the theoretical and experimental correlations among the six parameters, we proceed in the following way: we generate random sets of (a_0^0, a_0^2) or $(a_0^0, a_0^2, \theta_0, \theta_1)$, distributed according to the 2- or 4-dimensional gaussian obtained from the covariance matrix of the fit. We then fit the resulting distributions for the subthreshold parameters by gaussians, leading[4] to Table 1. $\rho_{\alpha\beta}$ denotes the correlation coefficient between α and β.

The slightly larger error bars of the "extended" fit, compared to the ones of the "global" fit, reflect the influence of the uncertainties in θ_0 and θ_1, which in the "global" fit are not explicitly taken into account. The differences in the central values between these two fits (although compatible within the errors) may be ascribed to the fact that the "extended" parametrization is not as accurate as the ACGL one, due to the fact that the former has to account for the dependence on two more variables. The column referring to the "scalar" fit should be understood as originating from a mixture of E865 data and χPT-based theoretical predictions that rely on assumptions about the size of $O(p^6)$ counterterms (see Sect. 7). For this reason the associated errors should not be interpreted in the strict statistical sense. The corresponding 1- and 2-σ ellipses in the $(\alpha - \beta)$ plane are drawn in Fig. 2.

[4] The phenomenological moments J_n^I are integrals of the $I = 0, 1, 2$ phase shifts from threshold to $\sqrt{s_2} = 2$ GeV. The solutions of the Roy equations are used for $s \leq s_0$, and experimental input is used above the $K\bar{K}$ threshold. An interpolation is necessary in the intermediate region $[s_0, 4M_K^2]$. We have observed a weak sensitivity of λ_1 and λ_2 on the interpolation prescription. On the other hand, the values of α and β are independent of this procedure

It is worth stressing that a rather small difference between a_0^0 and a_0^2 resulting from the scalar fit, on the one hand, and from the global and extended fits on the other hand, results in a more pronounced difference in the corresponding values of the subthreshold parameters α, β. Whereas the scalar fit (and the CGL prediction) is characterized by values of α close to (or smaller than) 1 and β well above 1.10, the global and extended fits lead to central values of $\alpha \sim 1.4$ and relatively smaller values of β. It will be shown elsewhere [23] that this qualitative difference finds its interpretation within the three-flavour analysis of $\pi\pi$ scattering together with other observables.

5 $N_f = 2$ Mass and decay constant Identities

In order to investigate the consequences of the results obtained so far for the parameters of the effective Lagrangian, we start with the Ward identity satisfied by the two-point function of the divergence of the axial current $\bar{u}\gamma_\mu\gamma_5 d$ and of its conjugate at zero momentum transfer. We isolate all LO (linear) and all NLO (quadratic) contributions in the quark mass $m = (m_u + m_d)/2$, and collect all $O(m^3)$ and higher order terms into the NNLO remainder δ:

$$F_\pi^2 M_\pi^2 = F^2 M^2 + \frac{M^4}{32\pi^2}(4\bar{\ell}_4 - \bar{\ell}_3) + F_\pi^2 M_\pi^2 \delta. \qquad (22)$$

Here

$$M^2 = 2mB, \qquad B = \Sigma(2)/F^2 \qquad (23)$$

are defined in the $SU(2) \times SU(2)$ chiral limit, keeping the strange quark mass at its physical value:

$$F = \lim_{m_u, m_d \to 0} F_\pi|_{m_s = \text{physical}}\,, \qquad (24)$$

$$\Sigma(2) = -\lim_{m_u, m_d \to 0} \langle \bar{u}u \rangle|_{m_s = \text{physical}}\,. \qquad (25)$$

A similar identity holds for the two-point function of axial minus vector currents, giving

$$F_\pi^2 = F^2 + \frac{M^2}{8\pi^2}\bar{\ell}_4 + F_\pi^2\varepsilon. \tag{26}$$

On the right hand side, all LO and NLO contributions are again explicitly shown, and all higher orders - $O(m^2)$ and higher - are included in the NNLO remainder ε. $\bar{\ell}_3$ and $\bar{\ell}_4$ are the standard $SU(2)\times SU(2)$ LEC's, which are scale-independent and exhibit logarithmic singularity in the chiral limit. They can be defined non-perturbatively, via the low-energy behaviour of the two-point functions that enter the Ward identities considered above. It may be useful to consider the NNLO remainders δ and ε in (22) and (26) as known, and to treat the mass and decay constant identities exactly, not performing any expansion. This avoids the use of perturbation theory when eliminating the order parameters M^2 and F^2 in favour of observable quantities. We will see later that, despite the fact that $\alpha-1$ need not be particularly small, this non-perturbative precaution is not absolutely necessary in the $N_f=2$ case. It will however, be fully justified in the case of three light flavours. In any case, the above method – which does not coincide either with the Standard or with the Generalized χPT – is completely meaningful no matter how large $\bar{\ell}_3$ or how small the condensate might be.

The fundamental order parameters, in appropriate units, the condensate and the decay constant defined as:

$$X(2) = \frac{2m\Sigma(2)}{F_\pi^2 M_\pi^2}\,, \quad Y(2) = \frac{2mB}{M_\pi^2}\,,$$
$$Z(2) = \frac{F^2}{F_\pi^2} = \frac{X(2)}{Y(2)}\,, \tag{27}$$

are related to the observables M_π, F_π, to the LEC's $\bar{\ell}_3$ and $\bar{\ell}_4$ and to the NNLO remainders δ,ε by the following identities:

$$Y(2) = \frac{2(1-\delta)}{1-\varepsilon+[(1-\varepsilon)^2 - 2\bar{\ell}_3\xi(1-\delta)]^{(1/2)}}\,, \tag{28}$$
$$X(2) = 1-\delta-(4\bar{\ell}_4-\bar{\ell}_3)\xi Y(2)^2/2\,, \tag{29}$$
$$Z(2) = 1-\varepsilon-2\bar{\ell}_4\xi Y(2)\,. \tag{30}$$

In the last three equations, we have denoted

$$\xi = \frac{1}{16\pi^2}\frac{M_\pi^2}{F_\pi^2}\,. \tag{31}$$

The $\pi\pi$ subthreshold parameters α and β can be expressed similarly. Reading the LO and NLO perturbative contributions to $F_\pi^2 M_\pi^2\alpha$ and to $F_\pi^2\beta$ from [31], one obtains the identities:

$$\alpha = 1-(1+3\bar{\ell}_3-4\bar{\ell}_4)\xi Y(2)^2/2+\delta_\alpha\,, \tag{32}$$
$$\beta = 1+2(\bar{\ell}_4-1)\xi Y(2)+\varepsilon_\beta\,. \tag{33}$$

It may be expected – at least for the moment – that the NNLO direct remainders δ_α and ε_β are not more important than the uncertainties in the determination of the parameters α and β from experimental data.

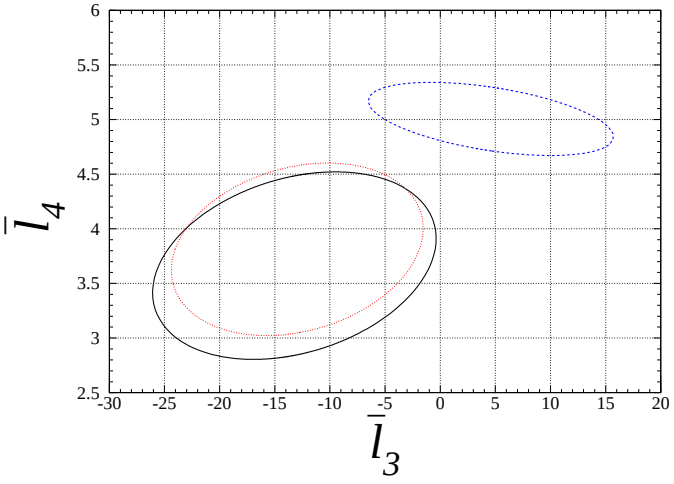

Fig. 3. 1-σ ellipse in the $\bar{\ell}_3-\bar{\ell}_4$ plane, from the fit "scalar" (blue, dashed ellipse) and our fits (black, solid for the "extended" and red, dotted for the "global"), using the linearized formulae

6 Determination of LEC's and order parameters

If we expand the previous expressions of α and β in powers of ξ, we obtain the following (linearized) expressions in term of the LEC's $\bar{\ell}_3$ and $\bar{\ell}_4$:

$$\alpha-\beta = 3\xi(1-\bar{\ell}_3)/2\,, \tag{34}$$
$$\beta-1 = 2\xi(\bar{\ell}_4-1)\,. \tag{35}$$

This is an excellent approximation, unless $\bar{\ell}_3$ or $\bar{\ell}_4$ become "too" large. However, even if one of them were large, the non-linear equations (32) and (33) of the previous section would still be exact identities; moreover, the definition of $\bar{\ell}_3$ and $\bar{\ell}_4$ in terms of two-point functions is independent of their magnitudes. We can use (34) and (35) to translate our determination of (α,β) into a 1-σ contour plot in the $\bar{\ell}_3-\bar{\ell}_4$ plane. In Fig. 3, we show three ellipses corresponding to those in the $\alpha-\beta$ plane displayed in Fig. 2 above.

If we use the formulae (28), (32) and (33), but now *without linearizing*, the previous ellipses are deformed, as shown in Fig. 4 (solid lines). The corresponding contours in the $X(2)-Z(2)$ plane are plotted in Fig. 5. Up to now, we have neglected the indirect remainders δ and ε as well as direct remainders δ_α and ε_β. In the case $N_f=2$, we expect these NNLO quantities to be less than 1%, since (22) and (26) are obtained by an expansion in powers of the *nonstrange* quark mass. This leads to a (small) additional broadening of the 1-σ regions, as seen in the plots with thinner lines in Figs. 4 and 5 (δ_α and ε_β are negligible compared to the present uncertainty in the parameters α and β).

It is clear from Fig. 4 that we obtain rather large and negative values of $\bar{\ell}_3$, compared to the standard expectation of 2.9 ± 2.4. This can be interpreted as a consequence of an important OZI-rule violating transition (1) leading

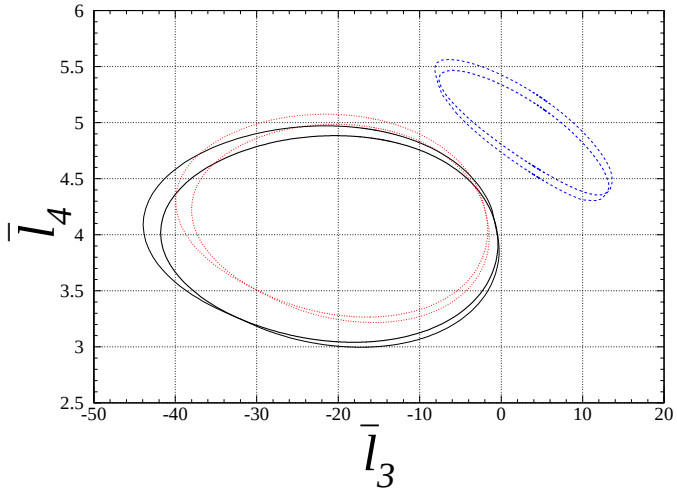

Fig. 4. 1-σ ellipse in the $\bar{\ell}_3 - \bar{\ell}_4$ plane, from the fit "scalar" (blue, dashed ellipse) and our fits (black, solid for the "extended" and red, dotted for the "global"), using the non-linearized formulae. The thinner lines indicate the domains allowed if $\varepsilon, \delta \leq 1\%$

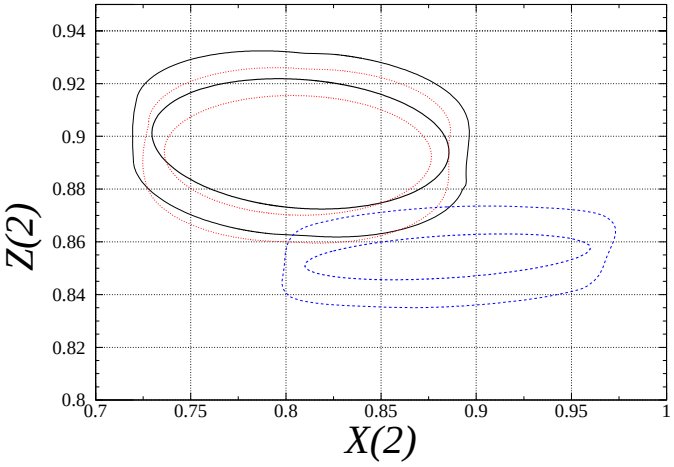

Fig. 5. 1-σ ellipse in the $X(2) - Z(2)$ plane, from the fit "scalar" (blue, dashed ellipse) and our fits (black, solid for the "extended" and red, dotted for the "global"). The thinner lines indicate the domains allowed if $\varepsilon, \delta \leq 1\%$

to a larger value of the $N_f = 3$, large-N_c suppressed constant $L_6^r(M_\rho)$, than usually assumed. Sum rule estimates of the latter [12,15] support this interpretation. Notice that the OZI rule is an important ingredient of the standard estimates of $\bar{\ell}_3$ [3]. We will return to this question elsewhere [23].

In Fig. 5, we see that the two-flavour GOR ratio $X(2)$ is constrained (at one sigma): $X(2) = 0.81 \pm 0.09$. In [32], this ratio has been theoretically analyzed, including the $O(p^6)$ double chiral logarithms of Generalized χPT, determining $X(2)$ as a function of $\alpha + 2\beta$ and other LEC's. A combination of the results of the latter analysis with the present (correlated) values for α and β leads to a range of values for $X(2)$ completely consistent with ours. Further examination of Fig. 5 shows that F/F_π is also limited to a rather narrow band, $(F/F_\pi)^2 = 0.90 \pm 0.03$. Let us mention that the difference seen in the (α, β) plane between the various fits reappears clearly here. The scalar fit (and the CGL prediction) favours larger values of $X(2)$ and lower values of $Z(2)$ than the global/extended fit.

7 Comments on the correlation between scattering lengths and the scalar radius of the pion

A relation between $2a_0^0 - 5a_0^2$ and the scalar radius of the pion based on two-loop χPT has been derived in [10, 29]. For the current value of the scalar radius $\langle r^2 \rangle_s = 0.61 \pm 0.04$ fm^2, this prediction results in the narrow strip in the $a_0^0 - a_0^2$ plane shown in [10] and reproduced here in Fig. 1. The accuracy of this prediction is not only conditional on the experimental error, but also on theoretical assumptions and "rules", which are a priori reasonable and natural, but not necessarily true.

First of all, these assumptions concern the estimates of the $O(p^6)$ corrections [20,29]. Although it is generally admitted that for certain observables (e.g. scattering lengths), these corrections could be enhanced, it is expected that for quantities receiving a weak contribution from $O(p^4)$ loops, the whole chiral expansion will rapidly converge. An example of this rule of thumb which is relevant for the present discussion is the quantity $C_1 - M_\pi^2 \langle r^2 \rangle_s / 3$, which does not contain $O(p^4)$ logarithms at all. (C_1 stands for a combination of subthreshold parameters defined in [29].) We shall argue that this fact does not prevent the corresponding $O(p^6)$ corrections from being relatively important. (An alternative "rule" is conceivable [23]: expand QCD correlation functions at kinematical points sufficiently distant from all Goldstone boson singularities. Such rule is a priori not less or more natural.) Next, it is usually assumed that $O(p^6)$ counterterms at a suitable scale can be estimated via the narrow resonance saturation [9,29,33]. In fact, already at $O(p^4)$ this assumption fails in channels where $1/N_c$ – corrections are large and/or the OZI-rule is strongly violated. This is what likely happens in the scalar channel, which is particularly relevant for the present discussion. Furthermore, the existing resonance estimates of $O(p^6)$ counterterms have been so far based on a "resonance effective Lagrangian $\mathcal{L}_{\rm res}$" involving (and missing) the same resonances with the same "minimal resonance couplings" as in [34], originally used to estimate the $O(p^4)$ LEC's. It has often been argued [35, 36] that additional non-minimal couplings are necessary to avoid conflicts with the QCD short-distance behaviour of two- and three-point functions, especially if the latter involve (pseudo)scalar currents. The estimates of the corresponding $O(p^6)$ counterterms r_1, r_2, r_3, r_4, r_S can be affected by these new resonance couplings. We shall return to the resonance estimates of the r_n's shortly.

Finally a remark should be made about the dispersive estimate of $\langle r^2 \rangle_s$ in [21], and the uncertainty related to it. The pion scalar form-factor and radius are not experimen-

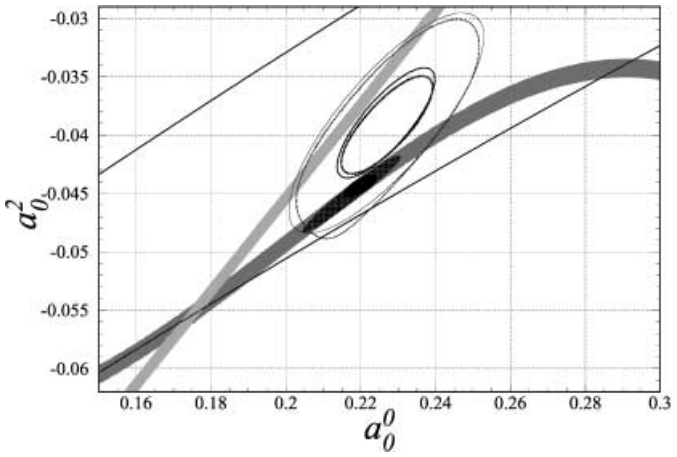

Fig. 6. Correlation (36) between a_0^0 and a_0^2, obtained from the relation between $2a_0^0 - 5a_0^2$ and the scalar radius of the pion. The shaded oblique band (yellow) corresponds to the $O(p^4)$ level [(36) with $\delta_a = 0$], using the dispersive estimate of [21]: $\langle r^2\rangle_s = 0.61 \pm 0.04$ fm^2. The shaded curved strip (cyan) represents the effect of $O(p^6)$ corrections δ_a according to the prediction of [10] using the same input value of $\langle r^2\rangle_s$. The contours correspond to fits using either the Roy solutions of [5] (red, dotted ellipse – "global") or our parameterization of the Roy solutions (black, solid ellipse – "extended"), with the errors of ACM(A) data enlarged as detailed in Appendix A. In each case, the thicker lines indicate the 1-σ ellipse, and the thinner ones the 2-σ contour. The other elements are identical to Fig. 1

tally measurable quantities – information about them can only come from indirect theoretical constructions. In contrast to the case of the (observable) vector form-factor, QCD does not restrict very much the high momentum behaviour of the scalar form-factor. It even does not guarantee that the latter satisfies an unsubtracted dispersion relation. Consequently, the dispersive evaluation of $\langle r^2\rangle_s$ suffers from a certain model dependence concerning the higher momentum contributions; this is usually not discussed in the literature. The quoted uncertainty should not be interpreted outside the framework of the model used in evaluating the scalar radius.

Most of these critical remarks are obviously not new. It might however be useful to keep them in mind when discussing the origin of the discrepancy between our model-free determination of scattering lengths from the data and the CGL narrow strip prediction [10]. The origin of the narrow strip (17) is more easily understood from (3) of [10]:

$$2a_0^0 - 5a_0^2 = \frac{3M_\pi^2}{4\pi F_\pi^2}\left(1 + \frac{1}{3}M_\pi^2\langle r^2\rangle_s + \frac{41}{12}\xi\right) + \delta_a \qquad (36)$$

$$= 0.57158 + 0.05541\left(\frac{\langle r^2\rangle_s}{0.61\ \text{fm}^2}\right) + \delta_a\,, \qquad (37)$$

where $\delta_a = O(m^3)$. It is worth stressing that the $O(p^6)$ contribution δ_a is essential for the numerical coherence of (36). If the $O(p^6)$ contribution δ_a is dropped, (36) reduces to the $O(p^4)$ low-energy theorem [31] relating $2a_0^0 - 5a_0^2$ and $\langle r^2\rangle_s$. This model-independent $O(p^4)$ relation is represented in Fig. 6 as a straight oblique band corresponding to the estimate of the scalar radius $\langle r^2\rangle_s = 0.61 \pm 0.04$ fm^2.

Table 2. Values of δ_a required for satisfying (36) and the estimate $\langle r^2\rangle_s = 0.61 \pm 0.04$ fm^2. The correlation between a_0^0 and a_0^2 has been taken into account to compute the error on $2a_0^0 - 5a_0^2$

	Scalar			Global		
a_0^0	0.218	$\pm$	0.013	0.2279	$\pm$	0.012
a_0^2	-0.0449	$\pm$	0.0033	-0.0382	$\pm$	0.0038
$2a_0^0 - 5a_0^2$	0.660	$\pm$	0.011	0.647	$\pm$	0.015
δ_a	0.033	$\pm$	0.012	0.020	$\pm$	0.015

In order to reproduce the prediction of [29]: $2a_0^0 - 5a_0^2 = 0.663 \pm 0.006$, either the scalar radius should be as large as 1.01 fm^2, or the $O(p^6)$ correction δ_a should move the $O(p^4)$ straight oblique band up to the curved strip along the bottom of the Universal Band, reproduced in Fig. 6 from [10]. If we believe the estimate $\langle r^2\rangle_s = 0.61 \pm 0.04$ fm^2, and if (36) should hold inside the scalar or the global ellipse, δ_a should take the values indicated in Table 2. The $O(p^6)$ correction amounts thus to 5% in the scalar case, and 3% in the global one.

This size of $O(p^6)$ corrections is consistent with general expectations. On one hand, NNLO contributions to "smooth" observables – typically, QCD correlation functions far from Goldstone boson singularities – are expected at 1% level (see the NNLO remainders δ and ε in Sect. 5). On the other hand, we expect an enhancement of higher-order corrections to infrared-singular "threshold quantities", such as scattering lengths [20,29,30]. Let us emphasize that, in order to reproduce the narrow strip of [10], the two-loop correction δ_a has to be known very precisely: this is no longer a matter of a model-independent low-energy theorem [31] nor of an accurate knowledge of $\langle r^2\rangle_s$. In particular, the CGL prediction [10] would be brought into agreement with the present determination of a_0^0 and a_0^2 by the "global" fit described in Sect. 3, if the $O(p^6)$ correction δ_a were reduced by factor 2, even if the scalar radius were not modified.

To understand the structure of the $O(p^6)$ correction δ_a, we follow [29] and write:

$$2a_0^0 - 5a_0^2 = \frac{3M_\pi^2}{4\pi F_\pi^2}C_1 + M_\pi^4\alpha_1 + O(M_\pi^8)\,. \qquad (38)$$

α_1 is a combination of phenomenological moments defined in (6.4) of [29]. C_1 collects polynomial coefficients in the chiral representation of the scattering amplitude. Its expansion in powers of m reads [29]:

$$C_1 = 1 + \frac{M_\pi^2}{3}\langle r^2\rangle_s + \frac{23\xi}{420} + \xi^2\Delta_1 + O(\xi^3)\,, \qquad (39)$$

where

$$\Delta_1 \equiv \frac{-71\tilde{L}^2}{12} + \tilde{L}\left\{ -\frac{40}{9}\tilde{\ell}_1 - \frac{80}{9}\tilde{\ell}_2 - \frac{5}{2}\tilde{\ell}_3 + 4\tilde{\ell}_4 + \frac{5393}{315}\right\}$$

$$-\tilde{\ell}_3\tilde{\ell}_4+\tilde{\ell}_4^2+\frac{1826}{315}\tilde{\ell}_1+\frac{3118}{315}\tilde{\ell}_2+\frac{79}{21}\tilde{\ell}_3-\frac{144}{35}\tilde{\ell}_4$$
$$-\frac{521}{252}\pi^2+\frac{24221}{3024}+\tilde{r}_2+4\tilde{r}_3-4\tilde{r}_4-2\tilde{r}_{S_2}\,, \qquad (40)$$

contains the $O(p^4)$ constants

$$\tilde{\ell_n}=\bar{\ell_n}-\tilde{L}, \qquad \tilde{L}=\log\frac{\mu^2}{M_\pi^2}\,, \qquad (41)$$

and the scale-dependent $O(p^6)$ counterterms

$$\tilde{r}_n=(4\pi)^4 r_n(\mu)\,. \qquad (42)$$

Comparing with (36), the $O(p^6)$ correction δ_a is seen to consist of two parts:

$$\delta_a=\delta_M+\delta_1\,. \qquad (43)$$

δ_M is essentially the phenomenological moment $M_\pi^4\alpha_1$ from which the leading infrared singularity has been subtracted:

$$\delta_M=M_\pi^4\alpha_1-4\pi\frac{353}{35}\xi^2\,. \qquad (44)$$

With the help of (6.8) of [29], one easily checks that in the chiral limit $m\to 0$ all $O(p^4)$ contributions on the right-hand side of (44) exactly cancel. In practice, however, $M_\pi^4\alpha_1$ is obtained by evaluating infrared singular sum rules using physical scattering lengths and not their values in the chiral limit. Consequently, the quantity δ_M is expected to be sensitive to the infrared enhancement of higher order corrections to the scattering lengths. One obtains:

$$M_\pi^4\alpha_1|_{\rm scalar}=0.0604\pm0.0054,$$
$$\delta_M|_{\rm scalar}=0.034\pm0.0054, \qquad (45)$$

$$M_\pi^4\alpha_1|_{\rm global}=0.0636\pm0.005,$$
$$\delta_M|_{\rm global}=0.037\pm0.005, \qquad (46)$$

for a_0^0 and a_0^2 inside the "scalar" and "global" ellipses respectively. The second part of the $O(p^6)$ correction δ_a is due to Δ_1:

$$\delta_1=12\pi\xi^3\Delta_1\,. \qquad (47)$$

As shown in (40), the latter depends on the $O(p^4)$ constants $\bar{\ell}_1,\bar{\ell}_2,\bar{\ell}_3,\bar{\ell}_4$ and on the counterterms $\tilde{r}_2,\tilde{r}_3,\tilde{r}_4,\tilde{r}_{S_2}$ describing $O(p^6)$ symmetry breaking effects in the scalar sector. The CGL prediction [10,29] of the strong correlation (17) between scattering lengths originates from a particular matching procedure worked out in [20], and from the resonance estimate of $O(p^6)$ counterterms [9,29,33], whose practical outcome is the fact that δ_1 is negligibly small and the whole two-loop correction δ_a reduces to the contribution δ_M as shown in (45). This conclusion is independent of the actual error in the dispersive estimate of the scalar radius $\langle r^2\rangle_s=0.61\pm0.04$ fm^2.

The smallness of δ_1 can indeed be justified within the framework defined by the assumptions summarized at the beginning of this section. To illustrate this point, let us concentrate first on a_0^0 and a_0^2 inside the ellipse resulting from the "scalar" fit. Choosing the scale $\mu=770$ MeV (δ_1 is scale-independent), we write

$$\delta_1=\delta_{CT}+\delta_\ell, \qquad (48)$$

where the counterterm part (at the scale μ) is:

$$\delta_{CT}=12\pi\xi^3(\tilde{r}_2+4\tilde{r}_3-4\tilde{r}_4-2\tilde{r}_{S2})\,, \qquad (49)$$

whereas the loop part δ_ℓ is given in terms of $O(p^4)$ constants $\bar{\ell}_1,\bar{\ell}_2,\bar{\ell}_3,\bar{\ell}_4$. We take [29]:

$$\bar{\ell}_1=-0.4\pm0.6, \qquad \bar{\ell}_2=4.3\pm0.1\,, \qquad (50)$$

and for $\bar{\ell}_3,\bar{\ell}_4$ we use the result of the "scalar" fit represented by the corresponding ellipse in Fig. 3. This leads to the estimate $\delta_\ell=0.0004\pm0.0083$. Using the resonance estimates of the r's [9,33,29] which are obtained according to the prescription mentioned above and assuming that the typical mass scale relevant in the scalar channel is $M_S=1$ GeV, one obtains $\delta_{CT}\sim0.00025$. The authors of [29] assume that this estimate ($\tilde{r}_1=-1.5,\tilde{r}_2=3.2,\tilde{r}_3=-4.2,\tilde{r}_4=-2.5,\tilde{r}_{S_2}=-0.7$) holds within a factor of 2. We can even relax this detailed estimate in favour of a more crude order of magnitude:

$$\tilde{r}_n=(4\pi)^4 r_n(\mu)\sim\pm\left(\frac{4\pi F_\pi}{M_S}\right)^4\,, \qquad (51)$$

which is expected to hold for $O(p^6)$ constants describing symmetry breaking effects in the scalar channel. The crucial point here is the dependence on the effective scalar mass M_S. As long as $M_S\sim1$ GeV, δ_{CT} will remain small: adding individual $\tilde{r}_n$ contributions randomly ($\tilde{r}_n\sim\pm1.8$), one gets in this case $\delta_{CT}\sim\pm0.0012$. The whole two-loop correction δ_a is then obtained by adding δ_M given by (45) with the estimates of δ_ℓ and δ_{CT}. One obtains $\delta_a=0.034\pm0.010$ in agreement with the value of δ_a required by the scalar fit and shown in Table 2.

We now return to the result of our paper indicating a deviation of the CGL narrow strip from experiment. Let us assume for the moment that the value of the scalar radius remains unchanged. Then, according to Table 2, the actual value of the two-loop correction $\delta_a=0.020\pm0.015$ is no longer saturated by $\delta_M=0.037\pm0.005$ and consequently δ_1 can no longer be negligible. The loop part δ_ℓ can be estimated as before. Taking the same values (50) of ℓ_1,ℓ_2 and using for ℓ_3,ℓ_4 the results of the global fit (see the corresponding ellipse on Fig. 3), one obtains in this case[5] $\delta_\ell=0.0096\pm0.0076$. This allows the extraction of the required value of the $O(p^6)$ counterterm combination δ_{CT}. Parametrizing the possible variation of the scalar radius by:

$$\langle r^2\rangle_s=0.61\ \text{fm}^2(1+\delta_r)\,, \qquad (52)$$

one obtains the final estimate for the combined effect of δ_{CT} and δ_r (our analysis does not allow us to disentangle these corrections):

$$\delta_{CT}+0.05541\cdot\delta_r=-0.0266\pm0.009\,. \qquad (53)$$

[5] All the above estimates of the loop part of Δ_1 can be reproduced by using its expression in terms of a_0^0 and a_0^2, which arises from the matching with the Roy equations' solutions

This means that both $O(p^6)$ contributions – the subtracted infrared singular moment δ_M and the symmetry breaking counterterms – are basically of the same order of magnitude. This is still consistent with the crude order of magnitude estimate of (51), provided the effective mass scale M_S characteristic of the scalar channel contributions is reduced by a factor 2: $M_S \sim 500$ MeV. This could indeed be a rather natural (though rough and qualitative) way how to account for the exceptional role of the $\pi\pi$ continuum and of the OZI-rule violation in the scalar channel. In this case, the estimate (51) leads to $|\delta_{CT}| \sim 0.019$, in qualitative agreement with (53), provided δ_{CT} is negative.

8 Conclusion

Low-energy $\pi\pi$ scattering has long been recognized as the golden observable to access the chiral structure of QCD vacuum. From one side the Roy equations allow a completely model-independent experimental determination of the two S-wave scattering lengths a_0^0 and a_0^2. Chiral symmetry can then be used to translate this information into knowledge of the LEC's of the chiral Lagrangian. In this paper we have followed these two steps using recent data on K_{e4} decays published by the E865 Collaboration. Contrary to previous analyses, we did not rely on any theoretical assumption about the correlation between a_0^0 and a_0^2, but rather supplemented the K_{e4} data with existing data in the $I = 2$ channel below 800 MeV. The result

$$a_0^0 = 0.228 \pm 0.012, \quad a_0^2 = -0.0382 \pm 0.0038 \qquad (54)$$

is compared with the theoretical relation between $2a_0^0 - 5a_0^2$ and the scalar radius of the pion [10] obtained in the standard two-loop χPT. If the dispersive determination of the latter, $\langle r^2 \rangle_s = (0.61 \pm 0.04)$ fm^2 is used, one finds a disagreement at the 1-σ level. It is possible to turn the argument around, and interpret this discrepancy as a measurement of $O(p^6)$ counterterms that contribute to the above theoretical relations. The latter come out larger than expected by the usual resonance saturation assumptions; this fact might be the manifestation of the exceptional status of the scalar channel, characterized by a strong $\pi\pi$ continuum and OZI rule violation.

The same conclusions are reached once we include in the Roy equations solutions the dependence on the phases at the matching point, $\sqrt{s} = 800$ MeV, θ_0 and θ_1. These two quantities are likely to represent the most important source of theoretical uncertainty for the Roy solutions, aside from the one on the driving terms. Our extended Roy solutions concretely parametrize the theoretical error on the phaseshifts, for a given value of a_0^0 and a_0^2.

Comparing the full two-loop standard χPT prediction for the two scalar scattering lengths [29], $a_0^0 = 0.220 \pm 0.005$ and $a_0^2 = -0.0444 \pm 0.0010$ with (54), one finds agreement for a_0^0, but a 1-σ discrepancy persists for a_0^2. This makes still more crucial the outcome of new precise experiments on $\pi\pi$, which are either planned [25] or ongoing [24]. In particular, more accurate K_{e4} data in the region of higher $s_{\pi\pi}$ could eventually allow a simultaneous determination of both a_0^0 and a_0^2 from a single set of data on $\delta_0^0 - \delta_1^1$. This might be preferable to the procedure adopted in the present paper, where E865 results are combined with the $\pi^+\pi^+$-production data of a different origin. Our result on a_0^0 (54) agrees with one of the two determinations of the isoscalar scattering length by the E865 collaboration [1] that does not use the narrow strip correlation between a_0^0 and a_0^2 as a theoretical input [10]. No determination of a_0^2 is reported in [1]. In this respect it is interesting to notice that the observed experimental correlation between a_0^0 and a_0^2 is positive and close to 1. The pionium lifetime experiments [24] cannot distinguish (a_0^0, a_0^2) pairs with the same $|a_0^0 - a_0^2|$, in particular the global and scalar fits which lead to $a_0^0 - a_0^2 = 0.266 \pm 0.010$ and 0.263 ± 0.010 respectively.

After determining the scattering lengths, we have studied the consequences for the $\pi\pi$ subthreshold parameters, by means of a matching procedure with the chiral amplitude. The influence of the uncertainty in θ_0 and θ_1 is only apparent in the parameters λ_1 and λ_2, whereas the others, in particular α and β, are practically independent thereof. These last two parameters are intimately related to the two main order parameters of $SU(2) \times SU(2)$ chiral symmetry, the quark condensate and the pion decay constant in the $SU(2)$ chiral limit, keeping the strange quark mass at its physical value. The result for the two-flavour GOR ratio $X(2) = 0.81 \pm 0.09$ corresponds to a large and negative central value for the LEC $\bar{\ell}_3 \sim -18$, to be compared with the standard expectation $\bar{\ell}_3 = 2.9 \pm 2.4$. Since this constant is rather sensitive to the OZI rule violating constants L_4 and L_6 of the three-flavour chiral Lagrangian, this conclusion seems to corroborate previous indications concerning the size of OZI rule violation [12,15] in the scalar channel, namely the value of L_6.

Finally, we would like to stress that, although crucial for understanding the pattern of $N_f = 2$ chiral symmetry breaking, $\pi\pi$ scattering alone does not tell us anything about the important question of the dependence of chiral order parameters on N_f. In particular it cannot be used to disentangle the "genuine" condensate of the purely massless theory, from the one "induced" by massive (but light) strange quark pairs. Nevertheless very accurate low-energy data on $\pi\pi$ scattering still represent an essential ingredient in a combined $SU(3) \times SU(3)$ analysis and forthcoming determination [23] of the three flavour condensate $\Sigma(3)$, the quark mass ratios and other "strange" features of the QCD vacuum. For this program, new low-energy $\pi\pi$ and πK scattering data are of obvious interest.

Acknowledgements. We would like to thank G. Colangelo, M. Knecht, B. Moussallam and H. Leutwyler for useful discussions and correspondence, J. Gasser for useful comments on the manuscript. Work partially supported by EEC-TMR contract ERBFMRXCT 98-0169 (EURODAPHNE). SD acknowledges partial support by PPARC, through grant PPA/G/S/1998/00530. LG acknowledges partial support from European Program HPRN-CT-2000-00149.

Appendix

A Treatment of errors for ACM(A) data

As discussed at the end of Sect. 3, it was proposed in [5] to take into account (unknown) systematic errors in method A of [6], by enlarging errors of ACM(A) solution in the following way. Consider for each energy bin the phase shift of solution A ($\delta_A \pm \Delta\delta_A$) and the one of solution B ($\delta_B \pm \Delta\delta_B$). The difference $|\delta_A - \delta_B|$ is supposed to reflect systematic errors of method A. The prescription advocated in [5] consists then in adding in quadrature this difference to the error $\Delta\delta_A$ quoted in [6]. The ACM(A) solution with enlarged errors is thus defined as:

$$\delta_A \pm \sqrt{(\Delta\delta_A)^2 + (\delta_A - \delta_B)^2} \tag{55}$$

The "global" and "extended" fits can be performed with these enlarged errors for ACM(A) phase shifts. The corresponding 1- and 2-σ contours for the S-wave scattering lengths are plotted in Fig. 6, while Table 3 summarizes the changes occurring to the various quantities considered in this paper. Let us mention that the nonlinear (28), (32) and (33) have been used to compute $\bar{\ell}_3$ and $\bar{\ell}_4$, and a contribution of the NNLO remainders $\delta, \varepsilon \leq 1\%$ is included in the error bars of $X(2)$ and F^2/F_π^2.

We see that enlarging errors for ACM(A) phase shifts slightly moves the global/extended contours in the (a_0^0, a_0^2) plane towards the bottom of the Universal Band. The effect is however marginal: the 1-σ discrepancy remains between the scalar and the global/extended fits, and the derived quantities $\bar{\ell}_3$, $\bar{\ell}_4$, $X(2)$ and F^2/F_π^2 are almost unchanged.

B Parametrization of the Roy solutions

In [5], the solutions of Roy equations have been described according to the Schenk parametrization (5). The Schenk parameters X_ℓ^I ($X = A, B, C, D, s$) are functions of the scattering lengths, a_0^0 and a_0^2, and the phase shifts at the matching point, $\delta_0^0(s_0) \equiv \theta_0$ and $\delta_1^1(s_0) \equiv \theta_1$. In [5], the Roy equations were solved for the particular choice of phase shifts at the matching point: $\theta_0 = 82.0°$ and $\theta_1 = 108.9°$, and the dependence on a_0^0 and a_0^2 of the parameters $X = A, B, C, D, s$ was parametrized according to (6).

We have followed the same procedure as in [5], with the only difference that θ_0 and θ_1 are explicitly treated as variables. After generating Roy solutions for $\theta_0 \in \{78.9°, 82.3°, 85.7°\}$ and $\theta_1 \in \{106.9°, 108.9°, 110.9°\}$, we then performed a fit of the form of (5), (6) and (8) with our solutions, in order to obtain the parameters a_i, b_i, c_i of (8). The Schenk parameters s_0^0, s_1^1 and s_0^2 are not parametrized in the form of (6), but are fixed by the condition at the matching point $\delta_\ell^I(s_0) = \theta_I$.

The parameters a_i are obtained by considering only the solution ($\theta_0 = 82.3°, \theta_1 = 108.9°$). The parameters b_i have then been obtained by fitting Roy solutions with $\delta\theta_0 \neq 0$ and $\delta\theta_1 = 0$, and the parameters c_i with $\delta\theta_0 = 0$ and $\delta\theta_1 \neq 0$. At each step, the fit has been performed at the level of the phase shifts, and not of the Schenk parameters, in order to ensure a smooth dependence on $(a_0^0, a_0^2, \theta_0, \theta_1)$. We have checked that this parametrization was adequate, even for solutions with both non-vanishing $\delta\theta_0$ and $\delta\theta_1$. The maximal gap between any solution and our parametrization is at most 1% in the $I = 0, 1, 2$ channels.

The coefficients resulting from the fit are expressed in units of M_π, and the phase shifts $\theta_{0,1,2}$ are in radians. For A_0^0 and A_0^2, all the coefficients a_i, b_i, c_i vanish, apart from:

$$A_0^0 : a_1 = a_2 = 0.225\,, \tag{56}$$

$$A_0^2 : a_1 = a_3 = -0.03706\,, \tag{57}$$

Table 3. Results of the global and extended fits, considering for ACM(A) phase shifts either the errors indicated in [6], or enlarged errors according to the prescription of [5]

	Global fit					
	ACM(A) errors			Enlarged errors		
a_0^0	0.228	±	0.012	0.227	±	0.012
a_0^2	-0.0382	±	0.0038	-0.0392	±	0.0041
χ^2	16.45			14.56		
α	1.381	±	0.242	1.334	±	0.252
β	1.081	±	0.023	1.088	±	0.024
$\rho_{\alpha\beta}$	-0.14			-0.25		
$\bar{\ell}_3$	-17.8	±	15.3	-14.1	±	15.0
$\bar{\ell}_4$	4.1	±	0.9	4.3	±	0.9
$X(2)$	0.81	±	0.07	0.82	±	0.07
$(F/F_\pi)^2$	0.89	±	0.02	0.89	±	0.03

	Extended fit					
	ACM(A) errors			Enlarged errors		
a_0^0	0.228	±	0.013	0.227	±	0.013
a_0^2	-0.0380	±	0.0044	-0.0389	±	0.0047
χ^2	16.48			14.59		
α	1.384	±	0.267	1.340	±	0.281
β	1.077	±	0.025	1.084	±	0.027
$\rho_{\alpha\beta}$	-0.23			-0.30		
$\bar{\ell}_3$	-18.5	±	16.7	-15.0	±	16.3
$\bar{\ell}_4$	4.0	±	0.9	4.2	±	1.0
$X(2)$	0.81	±	0.08	0.82	±	0.08
$(F/F_\pi)^2$	0.90	±	0.03	0.89	±	0.03

Par.	z_i	a_i	b_i	c_i
A_1^1	1	$.3617 \cdot 10^{-1}$	$-.1716 \cdot 10^{-2}$	$-.3860 \cdot 10^{-2}$
	2	$.1574 \cdot 10^{-1}$	$-.2448 \cdot 10^{-2}$	$-.3384 \cdot 10^{-3}$
	3	$.1057 \cdot 10^{-1}$	$-.1774 \cdot 10^{-2}$	$-.2510 \cdot 10^{-4}$
	4	$-.1782 \cdot 10^{-2}$	$-.1025 \cdot 10^{-1}$	$-.4312 \cdot 10^{-2}$
	5	$.2572 \cdot 10^{-3}$	$-.4649 \cdot 10^{-2}$	$-.1705 \cdot 10^{-2}$
	6	$-.2872 \cdot 10^{-3}$	$.1046 \cdot 10^{-2}$	$-.3467 \cdot 10^{-2}$
	7	$.8311 \cdot 10^{-2}$	$-.9152 \cdot 10^{-2}$	$-.3637 \cdot 10^{-2}$
	8	$-.2603 \cdot 10^{-2}$	$-.1489 \cdot 10^{-1}$	$.2188 \cdot 10^{-2}$
	9	$.1247 \cdot 10^{-2}$	$.7639 \cdot 10^{-3}$	$-.1340 \cdot 10^{-2}$
	10	$-.1186 \cdot 10^{-3}$	$.4371 \cdot 10^{-2}$	$.1128 \cdot 10^{-4}$

Par.	z_i	a_i	b_i	c_i
	1	.2482	$.4902 \cdot 10^{-1}$	$.1282 \cdot 10^{-1}$
	2	.1997	.1630	$-.3179 \cdot 10^{-3}$
	3	.1285	.1137	$.1640 \cdot 10^{-3}$
	4	$.1831 \cdot 10^{-1}$	−.1185	$.6305 \cdot 10^{-1}$
B_0^0	5	$.9970 \cdot 10^{-2}$	$-.6395 \cdot 10^{-2}$	$.1104 \cdot 10^{-1}$
	6	$.4846 \cdot 10^{-1}$	.3431	$-.1661 \cdot 10^{-1}$
	7	$-.3888 \cdot 10^{-2}$	−.1598	$.4322 \cdot 10^{-1}$
	8	$-.8912 \cdot 10^{-2}$	.5183	$-.3067 \cdot 10^{-1}$
	9	$-.4265 \cdot 10^{-2}$	$.4161 \cdot 10^{-1}$	$.8623 \cdot 10^{-2}$
	10	$-.3232 \cdot 10^{-2}$	−.1073	$.2976 \cdot 10^{-2}$

Par.	z_i	a_i	b_i	c_i
	1	$-.7257 \cdot 10^{-4}$	$-.1076 \cdot 10^{-4}$	$-.8750 \cdot 10^{-4}$
	2	$.2234 \cdot 10^{-3}$	$-.4577 \cdot 10^{-4}$	$-.8053 \cdot 10^{-5}$
	3	$.3718 \cdot 10^{-4}$	$-.3531 \cdot 10^{-4}$	$-.6497 \cdot 10^{-5}$
	4	$.2259 \cdot 10^{-4}$	$.2031 \cdot 10^{-4}$	$-.7306 \cdot 10^{-4}$
C_1^1	5	$.1216 \cdot 10^{-4}$	$-.2042 \cdot 10^{-4}$	$-.2856 \cdot 10^{-4}$
	6	$.4075 \cdot 10^{-4}$	$-.1625 \cdot 10^{-3}$	$-.1121 \cdot 10^{-3}$
	7	$-.1238 \cdot 10^{-4}$	$-.3676 \cdot 10^{-4}$	$-.2568 \cdot 10^{-4}$
	8	$.1103 \cdot 10^{-3}$	$-.3679 \cdot 10^{-3}$	$-.5010 \cdot 10^{-4}$
	9	$.3813 \cdot 10^{-4}$	$-.5706 \cdot 10^{-5}$	$.3202 \cdot 10^{-4}$
	10	$.3531 \cdot 10^{-4}$	$.1373 \cdot 10^{-3}$	$-.3439 \cdot 10^{-4}$

Par.	z_i	a_i	b_i	c_i
	1	$.1135 \cdot 10^{-3}$	$-.1685 \cdot 10^{-3}$	$-.6043 \cdot 10^{-3}$
	2	$-.2094 \cdot 10^{-2}$	$-.3429 \cdot 10^{-3}$	$-.5583 \cdot 10^{-4}$
	3	$-.8626 \cdot 10^{-3}$	$-.2467 \cdot 10^{-3}$	$-.2205 \cdot 10^{-4}$
	4	$.2911 \cdot 10^{-3}$	$-.8897 \cdot 10^{-3}$	$-.5793 \cdot 10^{-3}$
B_1^1	5	$.7343 \cdot 10^{-4}$	$-.4099 \cdot 10^{-3}$	$-.2258 \cdot 10^{-3}$
	6	$.2063 \cdot 10^{-3}$	$-.4832 \cdot 10^{-3}$	$-.6376 \cdot 10^{-3}$
	7	$.5294 \cdot 10^{-3}$	$-.6346 \cdot 10^{-3}$	$-.3879 \cdot 10^{-3}$
	8	$-.3372 \cdot 10^{-3}$	$-.2347 \cdot 10^{-2}$	$.9292 \cdot 10^{-5}$
	9	$-.1564 \cdot 10^{-3}$	$.1032 \cdot 10^{-4}$	$-.1169 \cdot 10^{-4}$
	10	$-.1301 \cdot 10^{-4}$	$.8137 \cdot 10^{-3}$	$-.1051 \cdot 10^{-3}$

Par.	z_i	a_i	b_i	c_i
	1	$-.7557 \cdot 10^{-2}$	$.2648 \cdot 10^{-2}$	$-.5166 \cdot 10^{-3}$
	2	$.3425 \cdot 10^{-1}$	$-.2038 \cdot 10^{-2}$	$.5412 \cdot 10^{-3}$
	3	$.2830 \cdot 10^{-1}$	$-.9686 \cdot 10^{-3}$	$.2995 \cdot 10^{-3}$
	4	$.3342 \cdot 10^{-2}$	$.5536 \cdot 10^{-2}$	$-.5538 \cdot 10^{-2}$
C_0^2	5	$.1391 \cdot 10^{-1}$	$.7956 \cdot 10^{-3}$	$-.2012 \cdot 10^{-2}$
	6	$.2375 \cdot 10^{-1}$	$.1775 \cdot 10^{-2}$	$.2675 \cdot 10^{-2}$
	7	$-.3024 \cdot 10^{-1}$	$-.1924 \cdot 10^{-1}$	$.6680 \cdot 10^{-4}$
	8	$-.9323 \cdot 10^{-1}$	$-.2108 \cdot 10^{-2}$	$.2173 \cdot 10^{-2}$
	9	$-.8813 \cdot 10^{-1}$	$.4251 \cdot 10^{-2}$	$-.2462 \cdot 10^{-2}$
	10	$-.2679 \cdot 10^{-1}$	$-.3504 \cdot 10^{-2}$	$.1984 \cdot 10^{-2}$

Par.	z_i	a_i	b_i	c_i
	1	$-.8567 \cdot 10^{-1}$	$-.5496 \cdot 10^{-2}$	$.1526 \cdot 10^{-2}$
	2	$-.1561 \cdot 10^{-1}$	$.1510 \cdot 10^{-2}$	$-.6254 \cdot 10^{-3}$
	3	$-.8722 \cdot 10^{-2}$	$.9679 \cdot 10^{-3}$	$.2538 \cdot 10^{-3}$
	4	$.9872 \cdot 10^{-2}$	$.1001 \cdot 10^{-1}$	$.2140 \cdot 10^{-1}$
B_0^2	5	$.2176 \cdot 10^{-1}$	$.3724 \cdot 10^{-2}$	$.3595 \cdot 10^{-2}$
	6	$.3338 \cdot 10^{-1}$	$-.1050 \cdot 10^{-1}$	$-.5945 \cdot 10^{-2}$
	7	$-.2051 \cdot 10^{-1}$	$.4012 \cdot 10^{-1}$	$.1157 \cdot 10^{-1}$
	8	$-.5171 \cdot 10^{-1}$	$.7078 \cdot 10^{-2}$	$.1593 \cdot 10^{-2}$
	9	$-.5929 \cdot 10^{-1}$	$-.6046 \cdot 10^{-2}$	$.1382 \cdot 10^{-2}$
	10	$-.2247 \cdot 10^{-1}$	$.4017 \cdot 10^{-2}$	$-.1490 \cdot 10^{-2}$

Par.	z_i	a_i	b_i	c_i
	1	$-.6396 \cdot 10^{-3}$	$.7978 \cdot 10^{-3}$	$.6667 \cdot 10^{-3}$
	2	$-.4143 \cdot 10^{-2}$	$.5649 \cdot 10^{-2}$	$-.5508 \cdot 10^{-4}$
	3	$-.3708 \cdot 10^{-2}$	$.5227 \cdot 10^{-2}$	$.1462 \cdot 10^{-3}$
	4	$-.4016 \cdot 10^{-2}$	$-.6414 \cdot 10^{-2}$	$-.8673 \cdot 10^{-3}$
D_0^0	5	$-.3159 \cdot 10^{-2}$	$-.3022 \cdot 10^{-2}$	$-.9427 \cdot 10^{-3}$
	6	$-.7352 \cdot 10^{-2}$	$.1584 \cdot 10^{-1}$	$.2274 \cdot 10^{-2}$
	7	$-.1305 \cdot 10^{-2}$	$-.1363 \cdot 10^{-1}$	$.3488 \cdot 10^{-2}$
	8	$-.4523 \cdot 10^{-2}$	$.1960 \cdot 10^{-1}$	$.1146 \cdot 10^{-2}$
	9	$-.4581 \cdot 10^{-2}$	$-.2917 \cdot 10^{-3}$	$-.1778 \cdot 10^{-2}$
	10	$-.1272 \cdot 10^{-2}$	$-.4082 \cdot 10^{-2}$	$.1184 \cdot 10^{-2}$

Par.	z_i	a_i	b_i	c_i
	1	$-.1652 \cdot 10^{-1}$	$.2246 \cdot 10^{-1}$	$.3320 \cdot 10^{-2}$
	2	$.3280 \cdot 10^{-2}$	$.5387 \cdot 10^{-1}$	$.9391 \cdot 10^{-4}$
	3	$.1127 \cdot 10^{-1}$	$.2911 \cdot 10^{-1}$	$.2303 \cdot 10^{-3}$
	4	$.1367 \cdot 10^{-1}$	.1198	$.9361 \cdot 10^{-2}$
C_0^0	5	$.1606 \cdot 10^{-1}$	$.5107 \cdot 10^{-1}$	$.1440 \cdot 10^{-3}$
	6	$.2990 \cdot 10^{-1}$	$-.1170 \cdot 10^{-1}$	$.1345 \cdot 10^{-2}$
	7	$-.5982 \cdot 10^{-2}$	$.9021 \cdot 10^{-1}$	$.1428 \cdot 10^{-1}$
	8	$.1923 \cdot 10^{-2}$	$.9601 \cdot 10^{-1}$	$-.4036 \cdot 10^{-2}$
	9	$.1106 \cdot 10^{-1}$	$.2148 \cdot 10^{-1}$	$-.1501 \cdot 10^{-2}$
	10	$.3809 \cdot 10^{-2}$	$-.2854 \cdot 10^{-1}$	$.2780 \cdot 10^{-2}$

Par.	z_i	a_i	b_i	c_i
	1	$.6607 \cdot 10^{-7}$	$-.1767 \cdot 10^{-6}$	$-.1271 \cdot 10^{-4}$
	2	$-.1750 \cdot 10^{-4}$	$-.5895 \cdot 10^{-5}$	$-.8847 \cdot 10^{-6}$
	3	$-.6507 \cdot 10^{-5}$	$-.5144 \cdot 10^{-5}$	$-.1517 \cdot 10^{-5}$
	4	$-.3851 \cdot 10^{-5}$	$.1657 \cdot 10^{-4}$	$-.7559 \cdot 10^{-5}$
D_1^1	5	$.4987 \cdot 10^{-6}$	$.2201 \cdot 10^{-5}$	$-.3089 \cdot 10^{-5}$
	6	$.1953 \cdot 10^{-6}$	$-.3159 \cdot 10^{-4}$	$-.1827 \cdot 10^{-4}$
	7	$-.2797 \cdot 10^{-4}$	$.3893 \cdot 10^{-5}$	$.1194 \cdot 10^{-5}$
	8	$.1604 \cdot 10^{-4}$	$-.5762 \cdot 10^{-4}$	$-.1570 \cdot 10^{-4}$
	9	$-.1183 \cdot 10^{-4}$	$-.9919 \cdot 10^{-6}$	$.9930 \cdot 10^{-5}$
	10	$-.7835 \cdot 10^{-5}$	$.2179 \cdot 10^{-4}$	$-.7949 \cdot 10^{-5}$

Par.	z_i	a_i	b_i	c_i
	1	$.1980 \cdot 10^{-3}$	$.1510 \cdot 10^{-3}$	$-.2527 \cdot 10^{-4}$
	2	$-.2572 \cdot 10^{-2}$	$-.5907 \cdot 10^{-4}$	$.1149 \cdot 10^{-4}$
	3	$-.2024 \cdot 10^{-2}$	$-.2137 \cdot 10^{-4}$	$.1067 \cdot 10^{-4}$
	4	$.1600 \cdot 10^{-2}$	$.5689 \cdot 10^{-3}$	$-.2189 \cdot 10^{-3}$
D_0^2	5	$.1790 \cdot 10^{-3}$	$.1280 \cdot 10^{-3}$	$-.7452 \cdot 10^{-4}$
	6	$.1228 \cdot 10^{-2}$	$-.3551 \cdot 10^{-4}$	$.9342 \cdot 10^{-4}$
	7	$.9168 \cdot 10^{-3}$	$-.7961 \cdot 10^{-3}$	$-.1405 \cdot 10^{-3}$
	8	$.4960 \cdot 10^{-2}$	$-.1981 \cdot 10^{-3}$	$.7174 \cdot 10^{-4}$
	9	$.5225 \cdot 10^{-2}$	$.2966 \cdot 10^{-3}$	$-.8173 \cdot 10^{-4}$
	10	$.1550 \cdot 10^{-2}$	$-.1694 \cdot 10^{-3}$	$.6938 \cdot 10^{-4}$

We determine s_0^0, s_1^1 and s_0^2 by the conditions:

$$\delta_0^0(s_0) \equiv \theta_0 \ , \qquad \delta_1^1(s_0) \equiv \theta_1 \ , \qquad \delta_0^2(s_0) \equiv \theta_2 \qquad (58)$$

where $\theta_2(a_0^0, a_0^2, \theta_0, \theta_1)$ is parametrized following (6) and (8), with the coefficients:

Par.	z_i	a_i	b_i	c_i
	1	$-.3160$	$.7038 \cdot 10^{-1}$	$-.2480 \cdot 10^{-1}$
	2	$-.2355$	$.2380 \cdot 10^{-1}$	$.6701 \cdot 10^{-2}$
	3	$-.2021$	$.1687 \cdot 10^{-1}$	$.5869 \cdot 10^{-2}$
	4	$.4885 \cdot 10^{-1}$	$.6057 \cdot 10^{-1}$	$-.2094 \cdot 10^{-1}$
θ_2	5	$-.1106 \cdot 10^{-1}$	$.2317 \cdot 10^{-1}$	$-.1128 \cdot 10^{-1}$
	6	$.8406 \cdot 10^{-2}$	$.7702 \cdot 10^{-1}$	$-.2254 \cdot 10^{-1}$
	7	$.3569 \cdot 10^{-2}$	.1531	.1103
	8	$.3021 \cdot 10^{-1}$	$.1027 \cdot 10^{-2}$	$-.4945 \cdot 10^{-2}$
	9	$.2762 \cdot 10^{-1}$	$.2859 \cdot 10^{-2}$	$-.1297 \cdot 10^{-1}$
	10	$.7229 \cdot 10^{-2}$	$.1513 \cdot 10^{-1}$	$.1340 \cdot 10^{-1}$

We have introduced the function $\theta_2(a_0^0, a_0^2, \theta_0, \theta_1)$ to improve the accuracy on s_0^2. The dependence of θ_2 on the S-wave scattering lengths and on the phases at the matching point is smoother than the analogous dependence of s_0^2. A direct fit of s_0^2 using the form of (6) and (8) would therefore induce a loss of accuracy, compared to the procedure we follow here.

References

1. S. Pislak et al. [BNL-E865 Collaboration], Phys. Rev. Lett. **87**, 221801 (2001)
2. L. Rosselet et al., Phys. Rev. D **15**, 574 (1977)
3. J. Gasser, H. Leutwyler, Annals Phys. **158**, 142 (1984)
4. S. M. Roy, Phys. Lett. B **36**, 353 (1971)
5. B. Ananthanarayan, G. Colangelo, J. Gasser, H. Leutwyler, Phys. Rept. **353**, 207 (2001) [arXiv:hep-ph/0005297]
6. W. Hoogland et al., Nucl. Phys. B **126**, 109 (1977)
7. M. J. Losty et al., Nucl. Phys. B **69**, 185 (1974)
8. M. Knecht, B. Moussallam, J. Stern, N. H. Fuchs, Nucl. Phys. B **457**, 513 (1995) [arXiv:hep-ph/9507319]
9. J. Bijnens, G. Colangelo, G. Ecker, J. Gasser, M.E. Sainio, Nucl. Phys. B **508**, 263 (1997) [Erratum-ibid. B **517**, 639] (1997) [arXiv:hep-ph/9707291]; Phys. Lett. B **374**, 210 (1996) [arXiv:hep-ph/9511397]
10. G. Colangelo, J. Gasser, H. Leutwyler, Phys. Rev. Lett. **86**, 5008 (2001) [arXiv:hep-ph/0103063]
11. S. Descotes, L. Girlanda, J. Stern, JHEP **0001**, 041 (2000) [arXiv:hep-ph/9910537]
12. B. Moussallam, Eur. Phys. J. C **14**, 111 (2000) [arXiv:hep-ph/9909292]
13. B. Moussallam, JHEP **0008**, 005 (2000) [arXiv:hep-ph/0005245]
14. S. Descotes, J. Stern, Phys. Lett. B **488**, 274 (2000) [arXiv:hep-ph/0007082]
15. S. Descotes, JHEP **0103**, 002 (2001) [arXiv:hep-ph/0012221]
16. L. Girlanda, J. Stern, P. Talavera, Phys. Rev. Lett. **86**, 5858 (2001) [arXiv:hep-ph/0103221]
17. H. Leutwyler, arXiv:hep-ph/0107332
18. N. H. Fuchs, H. Sazdjian, J. Stern, Phys. Lett. B **269**, 183. (1991) J. Stern, H. Sazdjian, N. H. Fuchs, Phys. Rev. D **47**, 3814 (1993) [arXiv:hep-ph/9301244]
19. M. Knecht, J. Stern, Published in 2nd DAPHNE Physics Handbook (169-190), L. Maiani, G. Pancheri, N. Paver Eds. [arXiv:hep-ph/9411253]
20. G. Colangelo, J. Gasser, H. Leutwyler, Phys. Lett. B **488**, 261 (2000) [arXiv:hep-ph/0007112]
21. J. F. Donoghue, J. Gasser, H. Leutwyler, Nucl. Phys. B **343**, 341 (1990)
22. B. Ananthanarayan, P. Büttiker, Eur. Phys. J. C **19**, 517 (2001) [arXiv:hep-ph/0012023]. B. Ananthanarayan, P. Buttiker, B. Moussallam, Eur. Phys. J. C **22**, 133 (2001) [arXiv:hep-ph/0106230]
23. S. Descotes, N.H. Fuchs, L. Girlanda, J. Stern, work in progress
24. B. Adeva et al., CERN proposal CERN/SPSLC 95-1 (1995); http://dirac.web.cern.ch/DIRAC/
25. R. Batley et al., CERN proposal CERN/SPSC 2000-3, CERN/SPSC/P253 add.3 (2000)
26. W. Ochs, MPI-PH-91-35 pi N Newslett. (1991) No. 3 25-42
27. S. D. Protopopescu et al., Phys. Rev. D **7**, 1279 (1973)
28. W. Hoogland et al., Nucl. Phys. B **69**, 266 (1974)
29. G. Colangelo, J. Gasser, H. Leutwyler, Nucl. Phys. B **603**, 125 (2001) [arXiv:hep-ph/0103088]
30. M. Knecht, B. Moussallam, J. Stern, N. H. Fuchs, Nucl. Phys. B **471**, 445 (1996) [arXiv:hep-ph/9512404]
31. J. Gasser, H. Leutwyler, Phys. Lett. B **125**, 325 (1983)
32. L. Girlanda, Phys. Lett. B **513**, 103 (2001) [arXiv:hep-ph/0104270]
33. J. Bijnens, G. Colangelo, P. Talavera, JHEP **9805**, 014 (1998) [arXiv:hep-ph/9805389]
34. G. Ecker, J. Gasser, A. Pich, E. de Rafael, Nucl. Phys. B **321**, 311 (1989)
35. B.Moussallam, J. Stern, in "Two photon physics from Daphne to LEP200, beyond", F. Kapusta, I.J. Parisi Eds. World Scientific, Singapore (1994); [arXiv:hep-ph/9404353]
36. M. Knecht, A. Nyffeler, Eur. Phys. J. C **21**, 659 (2001) [arXiv:hep-ph/0106034]